Elsevier Editorial System(tm) for Remote Sensing of Environment

Manuscript Draft

Manuscript Number:

Title: Seasonal and interannual dynamics of vegetation response to drought in a California urbanized area

Article Type: Research Paper

Keywords: Drought; Urban; California; Mediterranean climate; Landsat; AVIRIS; SPEI; NDVI; Surface temperature; Equivalent water thickness; Canopy water content; Eucalyptus; Coast live oak; Annual grass; Turfgrass

Corresponding Author: Mr. David L Miller,

Corresponding Author's Institution: University of California Santa Barbara

First Author: David L Miller

Order of Authors: David L Miller; Michael Alonzo; Susan K Meerdink; Michael A Allen; Christina L Tague; Dar A Roberts; Joseph P McFadden

Abstract: The effects of drought can manifest in vegetation across an array of physiological responses and time scales. In metropolitan areas, vegetation provides shading and cooling during hot and dry conditions, but these benefits can be reduced with drought. While many studies have evaluated interannual vegetation drought responses, seasonal responses have rarely been studied at the same time, especially in cities that regularly experience seasonal drought (e.g., in Mediterranean climates). Here, we evaluated seasonal and interannual drought responses across the dominant types of urban trees and grasses in the Santa Barbara, California, USA metropolitan area, using Landsat imagery acquired 2010-2019 and repeat Airborne Visible Infrared Imaging Spectrometer (AVIRIS) imagery acquired 2013-2015. To track vegetation types, we produced a random forest classification from 4 m AVIRIS-Next Generation (AVIRIS-NG) imagery acquired in June 2014 (overall accuracy = 86%; kappa = 0.85), thresholding to >90% pure pixels for most vegetation types in the coarser time series imagery. We monitored drought from Landsat imagery using the Normalized Difference Vegetation Index (NDVI) and the difference in land surface temperature (ΔLST) between vegetation and developed/impervious surfaces, as well as from AVIRIS using equivalent water thickness (EWT). NDVI was lower and ΔLST was closer to zero during drought years but they were seasonally correlated for only some vegetation types. Changes in EWT revealed seasonal adjustments by vegetation that were not readily apparent in the NDVI time series. Overall, EWT varied nonlinearly with NDVI within a single image and varied linearly when comparing median EWT and NDVI values across dates. However, the slopes of these relationships were dependent on vegetation type, suggesting that EWT and NDVI are unlikely to be linearly correlated across vegetation types. To attribute vegetation response to drought duration during different seasons, we examined the correlations of NDVI and ΔLST to the Standardized Precipitation Evapotranspiration Index (SPEI) calculated over a range of time spans. NDVI and ΔLST were most strongly correlated with SPEI during summer for most vegetation types, except for annual grass NDVI (winter).

Annual grass was generally correlated with SPEI at spans ≤12 months, whereas trees and turfgrass were commonly correlated with SPEI at spans >12 months in addition to seasonal time spans. This study describes interactions between drought duration and response in different types of urban vegetation, and demonstrates the benefits of using multiple, functionally-distinct remote sensing variables (NDVI, ΔLST, and EWT) in tandem to quantify changes in vegetation canopy condition during drought.

Suggested Reviewers: Sebastian van der Linden PhD
Professor, University of Greifswald
sebastian.linden@uni-greifswald.de
Professor van der Linden is an expert in mapping land cover through multispectral and hyperspectral remote sensing imagery, including urban areas and vegetation type distributions under changing climates.

Thomas Gillespie PhD
Professor, University of California Los Angeles
tg@geog.ucla.edu
Professor Gillespie is an expert in mapping and evaluating plant and tree species and richness, including several remote sensing studies in the Los Angeles urban area.

Darrel Jenerette PhD
Professor, University of California Riverside
darrel.jenerette@ucr.edu
Professor Jenerette is an expert on vegetation functioning and mapping in cities, including many remote sensing studies, and related work on energy balance and biodiversity in southern California and Arizona.

Opposed Reviewers:

Research Data Related to this Submission

There are no linked research data sets for this submission. The following reason is given:
Data will be made available on request

Highlights

We quantified response of urban trees and grasses to various time scales of drought.

NDVI and ΔLST had strongest correlations to SPEI during summer for most vegetation.

Unirrigated annual grass had strongest correlations with seasonal SPEI time spans.

Trees and turfgrass had strongest correlations with interannual SPEI time spans.

Vegetation EWT showed spring-to-fall decreases that were not as apparent in NDVI.

Title

Seasonal and interannual dynamics of vegetation response to drought in a California urbanized area

Authors

David L. Miller[a]*, Michael Alonzo[b], Susan K. Meerdink[c], Michael A. Allen[a], Christina L. Tague[d], Dar A. Roberts[a], Joseph P. McFadden[a]

a. Department of Geography, University of California, Santa Barbara, CA 93106, United States
b. Department of Environmental Science, American University, Washington, DC 20016, United States
c. Department of Geographical and Sustainability Sciences, The University of Iowa, Iowa City, IA 52242, United States
d. Bren School of Environmental Science and Management, University of California, Santa Barbara, CA 93106, United States
*Corresponding author: dlm@geog.ucsb.edu

Keywords

Drought; Urban; California; Mediterranean climate; Landsat; AVIRIS; SPEI; NDVI; Surface temperature; Equivalent water thickness; Canopy water content; Eucalyptus; Coast live oak; Annual grass; Turfgrass

Abstract

The effects of drought can manifest in vegetation across an array of physiological responses and time scales. In metropolitan areas, vegetation provides shading and cooling during hot and dry conditions, but these benefits can be reduced with drought. While many studies have evaluated interannual vegetation drought responses, seasonal responses have rarely been studied at the same time, especially in cities that regularly experience seasonal drought (e.g., in Mediterranean climates). Here, we evaluated seasonal and interannual drought responses across the dominant types of urban trees and grasses in the Santa Barbara, California, USA metropolitan area, using Landsat imagery acquired 2010-2019 and repeat Airborne Visible Infrared Imaging Spectrometer (AVIRIS) imagery acquired 2013-2015. To track vegetation types, we produced a random forest classification from 4 m AVIRIS-Next Generation (AVIRIS-NG) imagery acquired in June 2014 (overall accuracy = 86%; kappa = 0.85), thresholding to >90% pure pixels for most vegetation types in the coarser time series imagery. We monitored drought from Landsat imagery using the Normalized Difference Vegetation Index (NDVI) and the difference in land surface temperature (ΔLST) between vegetation and developed/impervious surfaces, as well as from AVIRIS using equivalent water thickness (EWT). NDVI was lower and ΔLST was closer to zero during drought years but they were seasonally correlated for only some vegetation types. Changes in EWT revealed seasonal adjustments by vegetation that were not readily apparent in the NDVI time series. Overall, EWT varied nonlinearly with NDVI within a single image and varied linearly when comparing median EWT and NDVI values across dates. However, the slopes of these relationships were dependent on vegetation type, suggesting that EWT and NDVI are unlikely to be linearly correlated across vegetation types. To attribute vegetation response to drought duration during different seasons, we examined the correlations of NDVI and ΔLST to the Standardized Precipitation Evapotranspiration Index (SPEI) calculated over a range of time

spans. NDVI and ΔLST were most strongly correlated with SPEI during summer for most vegetation types, except for annual grass NDVI (winter). Annual grass was generally correlated with SPEI at spans ≤12 months, whereas trees and turfgrass were commonly correlated with SPEI at spans >12 months in addition to seasonal time spans. This study describes interactions between drought duration and response in different types of urban vegetation, and demonstrates the benefits of using multiple, functionally-distinct remote sensing variables (NDVI, ΔLST, and EWT) in tandem to quantify changes in vegetation canopy condition during drought.

1. Introduction

Drought is a phenomenon that unfolds over time, affecting vegetation on time scales from rapid-onset "flash drought" events (Otkin et al., 2018) to megadroughts spanning years to decades (Williams et al., 2020). Vegetation has a variety of responses to drought, such as reductions in growth and primary production, adjustments in phenology, modifications in nutrient cycling, and increased mortality (Bréda et al., 2006; Van der Molen et al., 2011; Schlesinger et al., 2016; Trugman et al., 2018), but these effects do not necessarily take place at the same time scales across all types of vegetation, even within a single drought-affected region (e.g., Paz-Kagan and Asner, 2017; Rita et al., 2020). With anthropogenic influence increasing the intensity and likelihood of recent and future drought events (Diffenbaugh et al., 2015; Williams et al., 2015), it has become increasingly important to evaluate the impacts of drought at a range of temporal scales (Vicente-Serrano et al., 2010; 2013). This is especially needed in climatic regions that experience interannual droughts while regularly undergoing seasonal water limitations.

In Mediterranean climates, where the majority of precipitation falls during the winter and summers have little or no rainfall, vegetation regularly experiences both seasonal and interannual droughts, which are expected to intensify with climate change (Hanson and Weltzin, 2000). In

California, a Mediterranean climate covers much of the coastal zone of the state, which coincides with areas where most of the human population resides. Overlaid on this seasonally dry climate, during 2012-2016 California experienced one of the most severe droughts in its modern history (Lund et al., 2018). Given the increasing potential for future severe droughts in the state and Mediterranean regions in general (Diffenbaugh et al., 2015; Williams et al., 2015), there has been extensive research regarding how the 2012-2016 drought affected vegetation in natural and agricultural areas (e.g., Asner et al., 2016; Shivers et al., 2018; Okin et al., 2018; Dong et al., 2019), but the timing of the effects on vegetation in urban areas remains relatively understudied (e.g., Pincetl et al., 2019; Quesnel et al., 2019).

During the 2012-2016 drought, many cities in California reduced water use (Palazzo et al., 2017), with noticeable impacts on urban trees and turfgrass (Quesnel et al., 2019; Miller et al., 2020). During hot and dry conditions such as drought events, air and surface temperature cooling through shading and evapotranspiration represent important ecosystem services of urban vegetation (Shashua-Bar et al., 2009; Manickathan et al., 2018; Ziter et al., 2019). Concerns about maintaining these benefits as part of urban heat-reduction strategies (Norton et al., 2015) has led to increasing research into 'climate ready trees' (McPherson et al., 2018) and lawn-replacement programs (Pincetl et al., 2019). Despite this, the timing, magnitude, and persistence of drought effects on existing types of urban vegetation remain unclear. In natural areas adjacent to urbanized regions in California, trees and grasses in oak-savannas have differing responses to annual patterns of water availability, with grasses senescing during the summer and evergreen oak trees often maintaining green canopies through deeper water access (Gamon et al., 1995; Baldocchi et al., 2004). Additional differences in drought responses may occur in urbanized areas where much of the vegetation cover is irrigated over the summer (Litvak et al., 2017; Quesnel et al., 2019), there are many types of exotic and non-native vegetation (Alonzo et al., 2014; Avolio

et al., 2020), and there are potentially widely varying microclimatic effects, including those related to impervious surface cover (Leuzinger et al., 2010; Savi et al., 2015; Manickathan et al., 2018).

Accounting for the varying time scales of vegetation drought sensitivity in an urban area requires both a synoptic and a local view of changes, both of which can be characterized through remote sensing data. However, the inherent trade-offs in remote sensing data between spatial and temporal resolution make it challenging to both generate finely-resolved maps and track dense time series of urban vegetation with a single data source (van der Linden et al., 2018). Mapping in urban areas often requires high spatial resolution data to account for the fine-scale heterogeneity in urban materials (Cadenasso et al., 2007), and it benefits greatly from imaging spectroscopy (i.e., hyperspectral imagery) to effectively discriminate different types of vegetation and urban materials (Herold et al., 2004). The availability of these types of remote sensing data is primarily limited to airborne sensors with relatively few acquisitions, inhibiting the temporal resolution that is necessary to track drought effects (Ustin et al., 2004; van der Linden et al., 2018). Sufficiently dense temporal observations are more readily achieved with broadband spaceborne monitoring satellites such as Landsat or Sentinel-2 (van der Linden et al., 2018). The use of multiple forms of remote sensing data sources in tandem is therefore needed to investigate the temporal aspects of urban vegetation's response to drought.

The biophysical responses of vegetation to drought can vary with time. An initial plant response may be stomatal closure, leading to changes in leaf temperature and loss of leaf water content, while seasonal responses may include leaf senescence and, ultimately, mortality if the drought is sufficiently long and severe (Kozlowski et al., 1991; Bréda et al., 2006; Trugman et al., 2018). Different remote sensing measures will have different sensitivities to these plant responses. While greenness indices such as the Normalized Difference Vegetation Index (NDVI;

Rouse et al., 1973) are often used to track vegetation condition during drought (e.g., Vicente-Serrano et al., 2013; Okin et al., 2018; Dong et al., 2019), plants may express changes in canopy water content before significant changes in greenness and structure can be detected (Asner et al., 2004; Zarco-Tejada et al., 2012; Sims et al., 2014). Further, canopy or land surface temperature (LST) can be used as a proxy measure of vegetation evapotranspiration (Soer et al., 1980; Fisher et al., 2020) and, in urban areas, as a measure of vegetation cooling relative to impervious surfaces (ΔLST). Although it is strongly related to plant functioning, vegetation LST can be highly influenced by surrounding conditions and does not provide a direct measurement of canopy structure (Leuzinger et al., 2010; Meerdink et al., 2019b). Imaging spectrometer measurements of canopy water content, such as through equivalent water thickness (EWT), can provide a measure of leaf area index in dense canopies in addition to monitoring water (Roberts et al., 2004). Canopy water content measurements have been shown to effective in monitoring drought-induced canopy changes in California forests (e.g., Asner et al., 2016; Paz-Kagan and Asner, 2017), but are only rarely available at the temporal resolutions needed for tracking seasonal drought (e.g., Roberts et al., 1997; Dennison et al., 2003). By using complementary remote sensing data sets, studies can potentially capture changes that may not be readily apparent in a single index or measurement, more effectively constraining the timing of drought-induced changes in plant canopies.

Here, we leveraged multiple sources of remote sensing data to estimate the timing and influence of drought impacts on dominant vegetation cover types in the Santa Barbara, California, USA urbanized area. Specifically, we evaluated changes in prevalent tree (broadleaf trees, needleleaf trees, Eucalyptus, and oaks) and grass cover (annual grasses and turfgrass lawns) classes that may be expected to have distinct drought responses due to differing plant functional

strategies and water access. These classes occurred in sufficiently large patches to be tracked with coarser time series imagery. We took advantage of airborne imaging spectroscopy acquired over multiple seasons and years (Lee et al., 2015) as well as spaceborne satellite remote sensing time series (Dwyer et al., 2018) to examine the variable temporal effects of seasonal and interannual drought at a fine spatial scale across the metropolitan region. We addressed the following primary research questions:

1. How did the magnitude and timing of drought response compare across different vegetation cover types based on canopy greenness (NDVI), relative surface temperature (ΔLST), and canopy water content and leaf area (EWT)?
2. At which time spans (e.g., seasonal, interannual) are vegetation NDVI and ΔLST most correlated to drought based on the Standardized Precipitation Evapotranspiration Index (SPEI), and how does this vary by cover type and season?
3. How did EWT adjust seasonally in comparison to NDVI during this drought time series, and were there consistent linear relationships between EWT and NDVI across different vegetation types?

2. Methods

2.1. Study area

Our study area was 113 km^2 of the region surrounding and including Santa Barbara, California, USA (**Fig. 1**; 34.43° N, 119.75° W). The Santa Barbara urbanized area has a population of 196,000 (United States Census, 2012), and we defined our study area boundaries based on the availability of high resolution imaging spectroscopy data and a modified version of the United States Census boundary of the urbanized area. The climate is Mediterranean (Köppen

Csb), with the majority of the precipitation falling as rain in the winter months between November and April (mean annual air temperature 15 °C, mean annual precipitation 45 cm; National Centers for Environmental Information, 2019). The study area had persistent long-term drought conditions from early 2012 to early 2019, with reduced rainfall and high temperatures; the most severe drought conditions were from March 2014 to January 2017 (United States Drought Monitor, 2020).

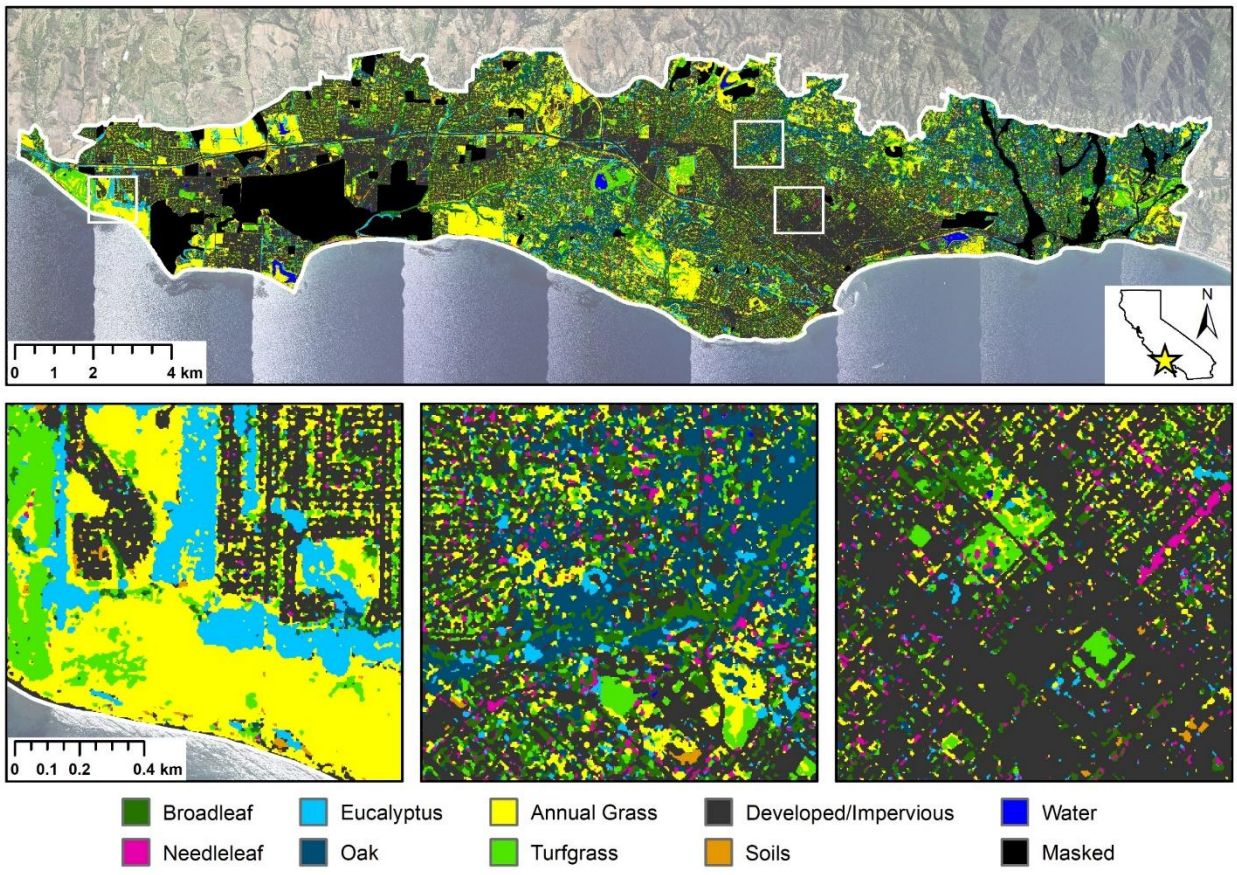

Fig. 1: Land cover classification map derived from 4 m AVIRIS-NG imagery acquired June 3, 2014, with a background of 1 m NAIP imagery from 2014. Top panel shows the full extent of the study area, with three example insets (white squares) ordered west to east, left to right: (Left) Open space with annual grasses, large remnant stand of Eucalyptus, and adjacent golf course and

residential neighborhoods; (Middle) Riparian area with oaks and other broadleaf trees surrounded by residential neighborhoods; (Right) Urban parks, dense residential, and commercial areas.

2.2. Land cover classification

To enable monitoring of different vegetation types within the study area during the drought, we produced a land cover classification from four flightlines of 4 m Airborne Visible Infrared Imaging Spectrometer - Next Generation (AVIRIS-NG) imagery acquired from a Twin Otter aircraft at 4 km altitude on June 3, 2014. This imagery provided sufficient spatial and spectral resolution to classify multiple dominant vegetation classes within our urban study area. AVIRIS-NG samples at 432 bands of spectral radiance at 5 nm spacing at approximately 350-2500 nm (Hamlin et al., 2011). The flightlines were radiance-calibrated and atmospherically corrected to surface reflectance by the NASA Jet Propulsion Laboratory (JPL). To provide greater internal consistency, we calibrated the AVIRIS-NG surface reflectance retrievals to ASD Field Spectrometer (Analytical Spectral Devices, Inc., Boulder, Colorado) measurements of a homogeneous, 25% reflectance flat white roof in Goleta, California (Thompson et al., 2015; Meerdink et al., 2019a). Each flightline was co-registered to 1 m National Agricultural Inventory Program (NAIP) orthophotos from 2014 using manually selected ground control points and Delaunay triangulation with nearest-neighbor resampling (NAD83, UTM Zone 11 N). The flightlines were mosaicked, giving precedence to the southern flightlines to favor the backscattering view geometry in overlapping areas. Bands adversely impacted by water vapor absorption were removed, leaving 312 bands. We applied continuum removal (Clark and Roush, 1984) on the remaining bands to mitigate the impacts of cross-track brightness and bidirectional reflectance distribution function effects between the mosaicked flightlines, as in Tane et al. (2018).

200 Land cover classes were selected to prioritize large patches of dominant urban vegetation
201 types that could be reliably tracked with coarser time series imagery (18 - 30 m spatial resolution)
202 and had potentially differing phenology and drought-response behaviors (**Table 1**). We evaluated
203 Eucalyptus and evergreen oak trees separately from the generic broadleaf tree class due to their
204 prevalence throughout the study area. The developed/impervious class included constructed
205 surfaces such as pavement and roofs, and we also mapped bare soil and inland open water bodies
206 due to their distinct spectral features. We created a combined training and validation dataset that
207 consisted of single cover type pixels using the AVIRIS-NG imagery, 1 m NAIP orthophotos from
208 2014, multiple dates of high resolution imagery in Google Earth, Google Street View, the City of
209 Santa Barbara's street tree database, and the tree species classification from Alonzo et al. (2016).
210 Each class sample size was initially set to ~250 single-pixel points, except for the small area
211 classes of soils and water. We randomly sampled this dataset (1850 pixel spectra total) without
212 replacement to develop training (70%) and validation (30%) data for each class.

Table 1: Classes and area estimates for the land cover classification, with non-representative polygons removed. Area and percentage of broadleaf trees exclude oaks and Eucalyptus, and in this study, broadleaf trees do not include Eucalyptus or oaks, unless specified otherwise.

Class Name	Description	Area (km^2)	Area (%)
Broadleaf	Broadleaf trees and shrubs, including native and non-native deciduous and evergreen, but not including Eucalyptus and oak (separate classes, see below)	13.19	12%
Needleleaf	Needleleaf trees and shrubs, primarily evergreen non-native	3.30	3%
Eucalyptus	Eucalyptus trees such as *Eucalyptus globulus*, a prominent broadleaf evergreen non-native tree	5.82	5%
Oak	Oak trees, predominantly *Quercus agrifolia*, a prominent broadleaf evergreen native tree	11.84	10%
Annual Grass	Annual grass and other low, primarily herbaceous, senesced vegetation in June 2014, likely non-irrigated	22.25	20%
Turfgrass	Turfgrass and other low, primarily herbaceous, green vegetation in June 2014, likely irrigated	9.08	8%
Developed/Impervious	Constructed urban surfaces including roads, roofs, and other impervious surfaces	45.25	40%
Soils	Bare soil surfaces and beach sand	1.35	1%
Water	Open water surfaces, ocean is excluded from classification	0.99	1%
TOTAL	Sum of all classes	113.07	100%

To create the land cover classification we used random forests, a nonparametric classification technique that generates an ensemble of decision trees and estimates the importance the input features (Breiman, 2001; Belgiu and Drăguț, 2016). We used a feature reduction technique ('varSelRF' package in R) to reduce the number of input continuum removed AVIRIS-NG bands from 312 to 88, similar to Tane et al. (2018). The 88 selected bands were input into a random forest model implemented in the 'ranger' package in R (Wright and Zeigler, 2017). We applied 'ranger' with 1000 trees, impurity importance, and otherwise default settings to generate the map. As a default, the number of features tried splitting at each node (mtry) was the square root of the number of input features (9).

After applying the random forest classifier to the AVIRIS-NG mosaic, we applied a 3x3 majority filter to smooth stray, misclassified pixels. To remove non-representative areas, we masked agricultural fields, marshes, and areas of major construction or redevelopment during the study time period. We also masked areas affected by the 2018 Montecito mudslide using polygons from Kean et al. (2019). For additional validation, we compared a subset of our land cover classification to the tree cover estimates for downtown Santa Barbara from Alonzo et al. (2016).

2.3. Landsat NDVI and ΔLST time series

We used all available Landsat Analysis Ready Data (ARD; Dwyer et al., 2018) scenes that were >30% clear for our study area between January 1, 2010 and December 31, 2019 (273 total). This included atmospherically corrected surface reflectance and thermal imagery from Landsat 5 Thematic Mapper (TM), Landsat 7 Enhanced Thematic Mapper + (ETM+), and Landsat 8 Operational Land Imager (OLI) and Thermal Infrared Sensor (TIRS). All Landsat imagery were reprojected to match the AVIRIS-NG classification's datum and projection (NAD83, UTM Zone 11N) using nearest-neighbor resampling; visual inspection on a subset of the Landsat scenes confirmed good spatial alignment of the 30 m Landsat imagery and the 4 m AVIRIS-NG classification. We calculated the NDVI for each Landsat scene (**Fig. 2A)**, and the Landsat 8 OLI NDVI was rescaled to approximate Landsat 7 ETM+ NDVI (equivalent to Landsat 5 TM NDVI) using Roy et al. (2016):

$$NDVI_{ETM+} = 0.0029 + 0.9589\, NDVI_{OLI} \quad \#(1)$$

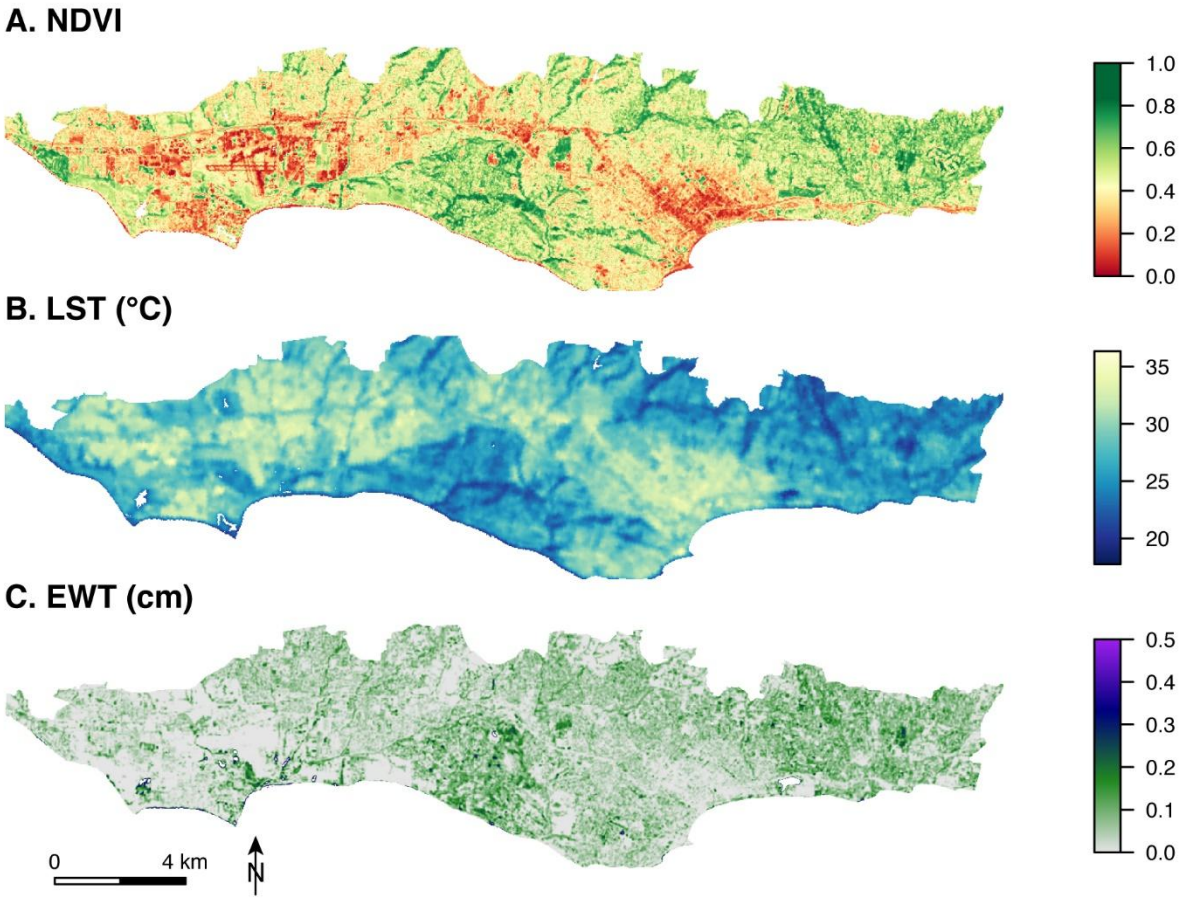

Fig. 2: Example images of A) NDVI and B) LST from Landsat 8 (April 8, 2015) and C) EWT from AVIRIS (April 16, 2015). EWT image has been smoothed for display clarity.

To investigate changes in land surface temperature (LST) due to its relationship with vegetation evapotranspiration and canopy shading, we used the USGS Landsat Provisional Surface Temperature Product (Cook et al., 2014) as a disaggregated 30 m estimation for LST (bias accuracy < 1 K, total uncertainty 2.5 K RMSE; Makalar et al., 2018) across all Landsat imagery (**Fig. 2B**). Since Landsat thermal bands have much coarser and variable pixel sizes (60-120 m, depending on the sensor) compared to the surface reflectance bands (30 m), there is likely a variable influence of surrounding cover types on the retrieved LST within a given 30 m pixel (Makalar et al., 2018). However, these data can provide an adequate approximation of LST for

the duration of our study time period and have been applied in other urban studies (e.g., Hoffman et al., 2020; Zhou et al., 2020). We restricted our analysis for both NDVI and LST to the same clear pixels based on the associated quality flags.

The 4 m AVIRIS-NG land cover classification was resampled to the 30 m Landsat grid by calculating the fraction within each 30 m Landsat pixel that was represented by each cover type. To characterize trends for different cover types, we extracted trends for all available pixels with >90% fractional cover for each cover type, except for needleleaf trees (>60%) because of their relatively small stand areas (supplemental material, **Table S1** and **Table S2**).

Values of NDVI and LST were aggregated to monthly median estimates for each cover type. To track the magnitude of relative cooling effect by vegetation type, we tracked LST at each month by subtracting the median LST for developed/impervious for each image from the median LST for each vegetation type (ΔLST). We then averaged ΔLST for each month, similar to studies of surface urban heat islands (e.g., Haashemi et al., 2016). Although we expected the magnitude of LST to change with impervious surface cover through an annual cycle (Yuan and Bauer, 2007), ΔLST provided a more broadly applicable metric for LST by accounting for weather-related, day-to-day variations in ambient temperatures. For example, we could more directly compare the relative cooling provided by vegetation in April 2015 vs. April 2016 using ΔLST than using absolute temperature.

2.4. Correlations of SPEI drought index and Landsat variables

To attribute the response of NDVI and ΔLST to seasonal and interannual drought, we examined their correlation with the Standardized Precipitation Evapotranspiration Index (SPEI; Vicente-Serrano et al., 2010). The SPEI is a drought index that quantifies differences from average water balance conditions based on precipitation and potential evapotranspiration; it is

standardized such that negative values are indicative of drier than average conditions while positive values are indicative of wetter than average conditions. Importantly for this study, SPEI can be calculated for a range of time scales, usually as an integrated span of months prior to the time point of interest, and so it can be representative of water balance conditions over shorter or longer time periods. For example, a SPEI span of 6 months quantifies relatively how much drier or wetter than normal conditions have been during the prior 6 months. The SPEI has been applied to Mediterranean ecosystems to evaluate the effects of drought on vegetation greenness, phenology, growth, and mortality (e.g., Barbeta et al., 2013; Ivits et al., 2014; Gouveia et al., 2017; Rita et al., 2020). As it included precipitation but not irrigation water use, which was not available across the study domain, SPEI provided a metric of relative meteorological drought to which distinct vegetation types may show differential response during our study time period.

We used all available SPEI spans (i.e., length of time included in the index for a given date) calculated for the US Historical Climatology Network station in Santa Barbara, California (34.4167° N, 119.6844° W) from the WestWideDroughtTracker (Abatzoglou et al., 2017). This included 1 to 12-month spans to represent the effects of seasonal-to-annual drought and time scales longer than 12 months, up to a maximum of 72 months, to represent interannual drought (examples of different spans are shown in supplemental material, **Fig. S1**). For each vegetation type, we calculated Pearson's correlation coefficient (R) for SPEI vs. NDVI, and SPEI vs. ΔLST, during different seasons: winter (December, January, February = DJF), spring (March, April, May = MAM), summer (June, July, August = JJA), and fall (September, October, November = SON). We estimated SPEI correlations for seasons, rather than individual months, to allow for 28-30 data points when computing correlations. For example, a 6-month SPEI span for winter would include the months of June to December, July to January, and August to February for December, January, and February, respectively.

2.5. EWT time series from AVIRIS

To investigate adjustments in plant water content based on equivalent water thickness (EWT), we used 18 m Airborne Visible Infrared Imaging Spectrometer (AVIRIS) flightlines that were acquired as part of the HyspIRI Preparatory Campaign during 2013-2015 (Lee et al., 2015). We used the 18 m AVIRIS imagery because it included repeat acquisitions over multiple seasons. AVIRIS measures spectral radiance at 10 nm spacing in the range of approximately 360-2500 nm (Green et al., 1998). We used a subset of the flightlines (31 total) that were processed to surface reflectance by JPL (Thompson et al., 2015) and Meerdink et al. (2019a) to capture spring, summer, and fall conditions for each year of acquisition, excluding lines with severe cloud contamination or technical issues in our study area (**Table 2**). In addition to the primary spatial coregistration from Meerdink et al. (2019a), the images were further co-registered to a 1 m NAIP mosaic from 2014 using Delaunay triangulation with nearest neighbor resampling (NAD83, UTM Zone 11 N) to constrain spatial alignment needed for the Santa Barbara urbanized area. Clouds were masked using manually drawn polygons. To exclude anomalous reflectance values due to low solar elevation angles, we masked the north-facing, shadowed slopes of the imagery acquired on November 25, 2013. To mitigate brightness discontinuities at higher off-nadir view angles towards the edges of the lines, lines at each date were mosaicked by averaging co-located pixels in overlapping flightlines using the 'mosaic' function in the R 'raster' package.

Table 2: Dates (Year.Month.Day) of AVIRIS flightlines (FL##) from the HyspIRI Preparatory Campaign's Santa Barbara Box used in this study, derived from Meerdink et al. (2019a). Flightlines included in this study are marked with 'x' and excluded or missing lines are marked with 'NA.'

Date	FL05	FL06	FL07	FL08
2013.04.11	x	x	x	x
2013.06.06	NA	x	NA	x
2013.11.25	NA	x	x	x
2014.04.16	x	x	x	x
2014.06.04	NA	NA	x	x
2014.08.29	x	x	x	x
2015.04.16	x	x	x	x
2015.06.02	x	x	x	x
2015.08.24	x	x	x	x

We evaluated changes in plant leaf water across all vegetation types during the drought by calculating EWT (**Fig. 2C,** Green et al., 1993; Roberts et al. 1997). EWT estimates the depth of liquid water, as described by Beer-Lambert Law, needed to approximate the shape of a measured vegetation spectrum. We used EWT as opposed to water-related vegetation indices because of the insensitivity of EWT to the varying solar zenith angles in our AVIRIS time series (Dennison et al., 2003; Cheng et al., 2006), although other vegetation indices may have stronger relationships to canopy water content (e.g., Serrano et al., 2000). Canopy water content and live fuel moisture estimated by EWT has been used multiple studies investigating the effects of drought on vegetation (e.g., Dennison et al., 2003; Asner et al., 2016; Paz-Kagan and Asner, 2017). We calculated EWT by minimizing the sum of squared differences by wavelength between the measured surface reflectance and estimated liquid water absorption:

$$minimize \sum_{\lambda=850\,nm}^{1100\,nm} (\rho_\lambda - be^{-t\alpha_\lambda})^2 \#(2)$$

where ρ_λ is the measured atmospherically-corrected surface reflectance at each wavelength, α_λ is liquid water absorption (cm^{-1}) at each wavelength, t is EWT (cm), and b is a scaling offset parameter. The variables t and b were adjusted with a nonlinear optimization routine ('optim' function in R, method = "L-BFGS-B"; Byrd et al., 1995) with the constraint that $t \geq 0$.

We estimated EWT for each AVIRIS image mosaic, including all bands between 850 and 1100 nm except the water vapor band at 928 nm, and we validated our EWT estimates using field-collected leaf water, leaf area, and spectra from Meerdink et al. (2016). To compare response in EWT to response in Landsat NDVI through the drought with matching pixel sizes and acquisition dates, we produced simulated Landsat 5 TM NDVI from the AVIRIS image mosaics by convolving the AVIRIS bands to Landsat 5 TM bands with spectral response functions in ENVI 5.2 Classic (L3Harris Geospatial, Broomfield, Colorado). Similar to the Landsat time series data extraction, we aggregated the 4 m AVIRIS-NG land cover classification to fractional cover estimates within the 18 m AVIRIS time series grid and extracted available pixels with >90% cover of a given vegetation cover type from each date of the AVIRIS EWT and simulated Landsat NDVI time series (supplemental material, **Table S3 and S4**). We then compared changes in time of these two variables for available AVIRIS dates. Specifically, we plotted all available EWT and NDVI values against each other to assess their overall relationship for different vegetation types, and we produced linear regressions across dates to evaluate the similarities or differences in response of EWT and NDVI for different vegetation types.

3. Results

3.1. Land cover classification

The land cover classification from the 4 m AVIRIS-NG imagery and the random forest classifier is shown in **Fig. 1**. The overall accuracy and kappa of the land cover classification were 86% and 0.85, respectively (**Table 3**). Using all validation sample points, the mean user's accuracy (UA) was 88% and the mean producer's accuracy (PA) was 86%; weighted by final land cover class areas, mean UA was 85% and mean PA was 91%. Most of the land cover classes had accuracies >80%, with the exception of the more diverse broadleaf tree (UA = 75%, PA = 69%) and needleleaf tree classes (UA = 84%; PA = 77%), which were misclassified as other vegetation types more often than other classes. Variable importance from the random forest model is shown in the supplemental material (**Fig. S2**). The full 113 km^2 study extent had 30% tree cover, 40% developed or impervious surfaces, 20% annual grass, and 8% green turfgrass (**Table 2**). Of the total tree cover, 90% was all types of broadleaf trees including Eucalyptus (17%), oaks (~35%), and other broadleaf trees (~39%), whereas only 10% was needleleaf trees. Our classification's cover estimates for oak, needleleaf, and broadleaf trees, with or without Eucalyptus and oak trees included, were all similar to estimates from Alonzo et al. (2016) in a subset of the study area in downtown Santa Barbara (22 km^2, supplemental material, **Table S5**).

Table 3: Error matrix for land cover classification. Overall accuracy = 86%, kappa = 0.85. Note that unequal class sizes were necessary to rebalance the relative influence of different classes within the random forest model.

		Reference										
		Broadleaf	Needleleaf	Eucalyptus	Oak	Annual Grass	Turfgrass	Dev./Imp.	Soils	Water	TOTAL	User's Accuracy
Prediction	Broadleaf	62	11	2	5	0	3	0	0	0	83	75%
	Needleleaf	6	46	3	0	0	0	0	0	0	55	84%
	Eucalyptus	3	0	69	0	0	0	0	0	0	72	96%
	Oak	6	0	1	51	0	0	0	0	0	58	88%
	Annual Grass	4	1	0	1	74	4	0	2	0	86	86%
	Turfgrass	3	0	0	2	1	68	0	0	0	74	92%
	Developed/Impervious	6	2	0	1	0	0	73	4	2	88	83%
	Soils	0	0	0	0	0	0	2	24	0	26	92%
	Water	0	0	0	0	0	0	0	0	13	13	100%
	TOTAL	90	60	75	60	75	75	75	30	15	555	
	Producer's Accuracy	69%	77%	92%	85%	99%	91%	97%	80%	87%		

3.2. Landsat NDVI and ΔLST time series

We evaluated seasonal and interannual time series of vegetation condition based on Landsat NDVI and ΔLST during 2010-2019, comparing the changes within individual years as well as the conditions for the same months across different years (**Fig. 3**).

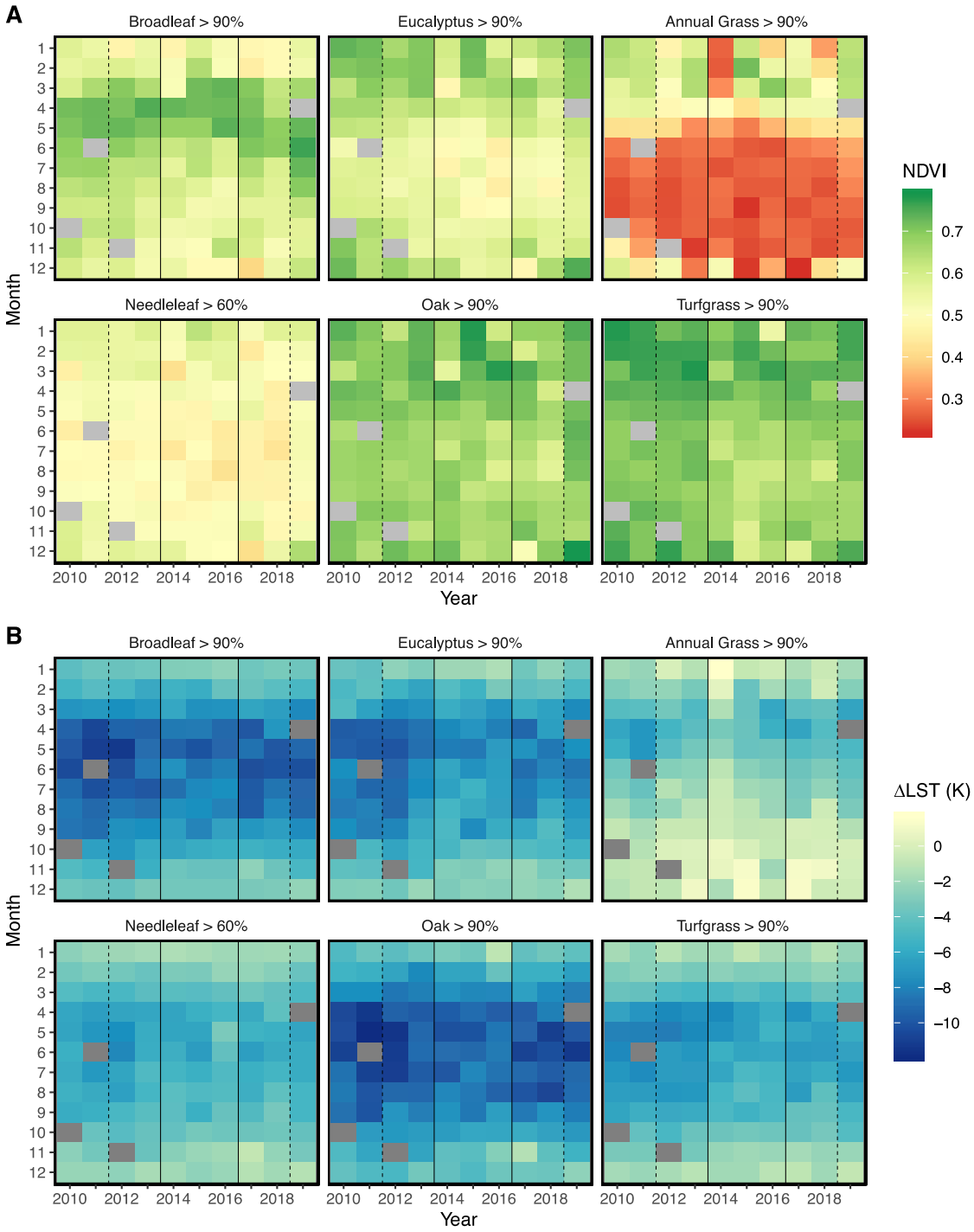

393

394 **Fig. 3**: Landsat NDVI and ΔLST observations. A) Median NDVI aggregated monthly (vertical

395 axis) for each year (horizontal axis) for each vegetation cover class. B**)** Median ΔLST aggregated

396 monthly (vertical axis) for each year (horizontal axis) for each vegetation cover class. On both A

and B, gray cells indicate missing observations, and black vertical lines describe approximate boundaries of drought condition from United States Drought Monitor (2020) for the Santa Barbara, California urbanized area: between dashed lines (2012-2013, 2017-2018) is "Abnormally Dry" to "Extreme Drought;" between solid lines (2014-2016) is "Exceptional Drought," the most severe drought category.

The major urban vegetation types exhibited distinct temporal patterns in NDVI in response to drought. Broadleaf trees had signals typical of winter deciduous trees, with highest NDVI values in the spring and, in wetter years, early summer. However, broadleaf NDVI declined during August and September during 2015 and 2016, likely related to earlier senescence during peak drought years. Needleleaf trees showed moderate NDVI values throughout the year (min. = 0.41, max. = 0.65), with slightly higher values in the winter and declines during the summers of 2016-2019, a later response than the broadleaf trees. The lower overall values of NDVI for needleleaf trees were likely related to mixed image pixels containing developed/impervious surfaces because needleleaf trees were sampled in patches as low as 60% fractional cover due to the rarity of large patches. Eucalyptus had its highest NDVI values in winter, but also showed severe winter reductions in NDVI during drought years. In general, NDVI values for Eucalyptus from 2013 onward were likely influenced by understory annual grasses as the Eucalyptus tree canopy declined during the drought. By comparison, the evergreen oaks, which do not experience a reduction in canopy cover, had relatively constant NDVI, with only slight declines during summer in 2016-2018 and some year-to-year variation in winter NDVI, with particularly low values in winter 2014. Annual grass showed high seasonal variability, with relatively high NDVI (~0.6) in wetter winters and very low NDVI (~0.3) in summer, responding to seasonal shifts from winter precipitation to summer drought. However,

annual grass NDVI remained very low during winter 2014 and, to a lesser degree, 2018, and the low summertime values extended later into the fall during drought years (2013-2017). Turfgrass, due to irrigation, overall had relatively consistent NDVI throughout all years and had higher wintertime values, but also had relative declines during summer in peak drought years (2014-2016).

To account for differences in weather in each image acquisition, we tracked vegetation ΔLST as the difference between median vegetation LST and median developed/impervious LST within each image; more negative values of ΔLST indicate cooler vegetation relative to developed/impervious surfaces. In general, ΔLST was closest to zero during winter for all vegetation cover types likely due to low solar elevation angles and greater shadowing of urban paved surfaces. The most negative values of ΔLST were from April to September when paved surfaces had more direct insolation and were relatively less shaded. Broadleaf, Eucalyptus, and oak showed stronger relative cooling during summer for the pre-drought years 2010-2011 (mean = -9.4 K, -8.2 K, -9.7 K, respectively) that was reduced in magnitude during the drought in 2014-2016 (-7.8 K, -6.1 K, -8.7 K, respectively). In general, there was a weakening of ΔLST vegetation cooling during summer in 2014-2016 (all vegetation mean = -5.8 K) compared to 2010-2011 (-7.2 K). In particular, annual grass had ΔLST values close to 0 throughout 2014 (annual mean = -0.6 K) compared to 2010-2011 (-5.7 K), with only slight cooling in the spring 2014 (-2.7 K), which was more similar to spring 2010-2011 (-3.0 K). The ΔLST medians for nearly all vegetation types were always negative (i.e., cooler than paved surfaces) for all months and years, except for annual grass during the late fall and winter of several drought years.

While we anticipated more leaf cover (higher NDVI) would be correlated with cooler relative surface temperatures (lower ΔLST), this relationship was not universal across vegetation types (**Fig. 4**). Broadleaf trees and annual grass showed the strongest negative correlations

(Pearson's R = -0.76 and -0.51, respectively) between seasonal changes in NDVI and ΔLST. Broadleaf trees had the most linear response likely because they are deciduous, whereas annual grass showed a distinct separation between winter and spring because of its wintertime greening, with relative cooling being delayed. Needleleaf trees had an unexpectedly positive correlation (R = 0.44) between seasonal changes in NDVI and ΔLST, perhaps due to the abundance of impervious surfaces being the primary influence upon changes in ΔLST in these more mixed pixel samples, or the greater presence of winter shadows increasing near-infrared reflectance relative to red. Eucalyptus, oaks, and turfgrass did not show great variability in seasonal NDVI as compared to the observed changes in ΔLST, although Eucalyptus had a weak positive correlation (R = 0.25), perhaps also due to wintertime shadowing. In general, due to seasonal drought and the presence of evergreen vegetation in this study area during this time period, vegetation greening did not necessarily imply more relative cooling through an annual cycle.

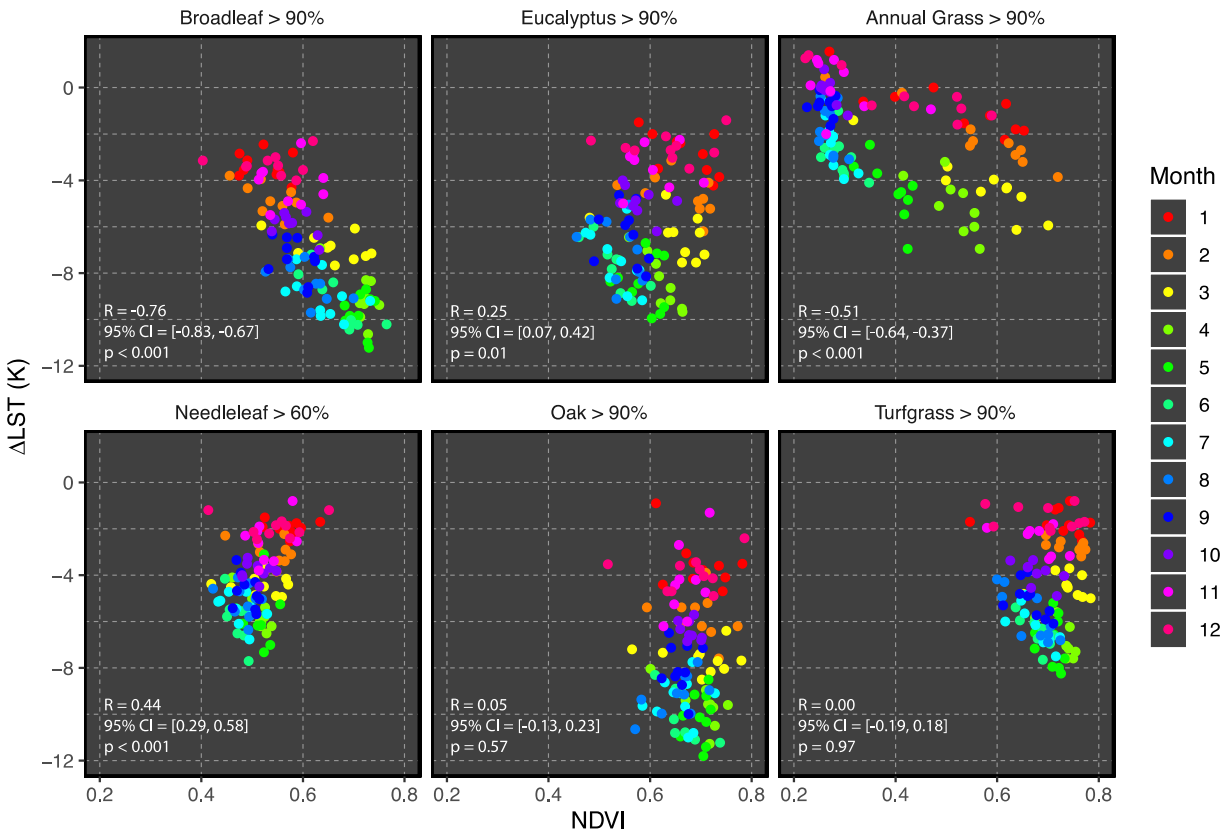

458

459 **Fig. 4**: Landsat median NDVI vs. median ΔLST for each vegetation cover type, plotted with

460 different colors for each month for all years. Pearson's correlation R values, 95% confidence

461 intervals, and p-values are shown in lower left of each plot.

462

463 3.3. Landsat NDVI and ΔLST correlations with SPEI spans

464 We examined the correlations of SPEI at different time spans to NDVI and ΔLST,

465 respectively, to assess the impact of drought duration on vegetation response. Because SPEI is

466 negative during drier conditions and positive during wetter conditions, in general, NDVI was

467 positively correlated with SPEI and ΔLST was negatively correlated with SPEI. We compared

468 the strength of these correlations during different seasons. At the same time, because SPEI at

469 different spans summarizes conditions integrated over a range of time, we examined seasonal

droughts with SPEI spans ≤12 months and interannual droughts with SPEI spans >12 months. Both NDVI and ΔLST showed distinct correlations with SPEI at different spans (i.e., drought duration) for different seasons of the year, which often varied by vegetation cover type (**Fig. 5**). The highest correlations for each vegetation type are shown in **Table 4**.

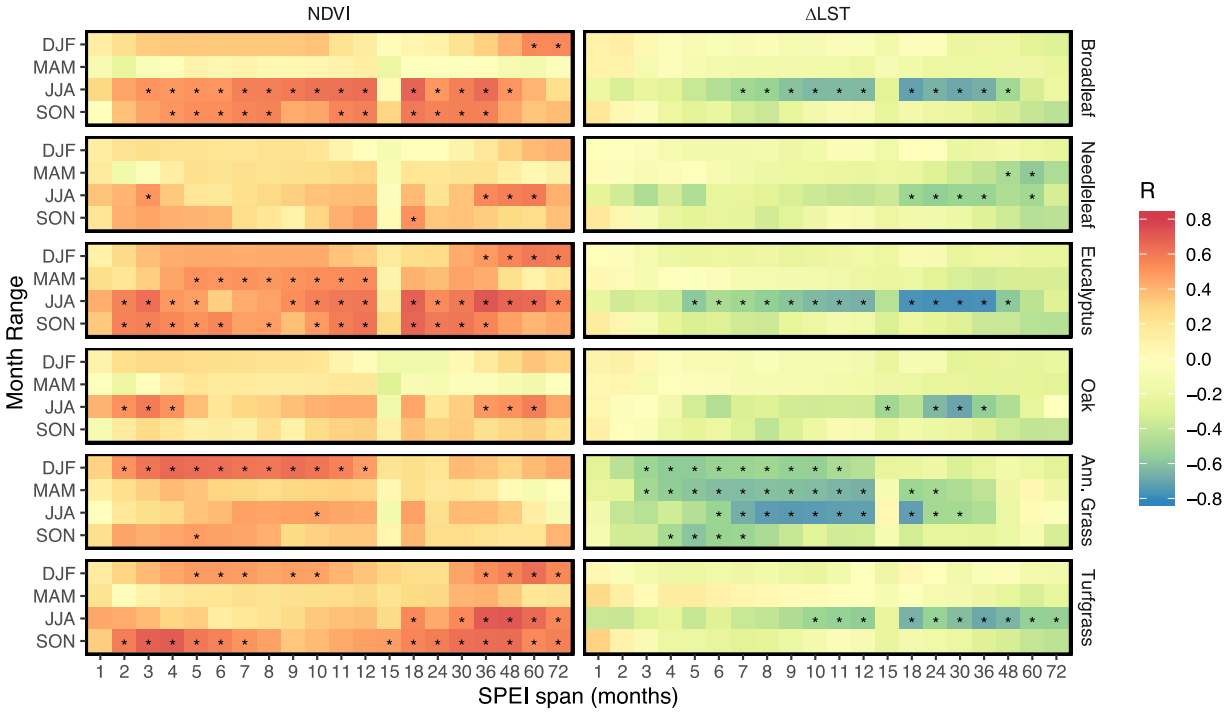

Fig. 5: Pearson's R correlations between SPEI span (x) and NDVI (left column) or ΔLST (right column) for each vegetation cover type (row blocks, with right side labels). Each cover type's correlations are tracked by season (y): winter = DJF, spring = MAM, summer = JJA, and fall = SON. Cells with significant correlations ($p < 0.01$) are marked with *. Note that the x-axis is not years, as in **Fig. 3**.

Table 4: Highest magnitude Pearson's R correlations between SPEI span and NDVI (left columns) or ΔLST (right columns) for each vegetation cover type for different seasons: winter = DJF, spring = MAM, summer = JJA, and fall = SON.

	NDVI			ΔLST		
	R	Season	SPEI Span (months)	R	Season	SPEI Span (months)
Broadleaf	0.69	JJA	18	-0.71	JJA	18
	0.65	JJA	36	-0.69	JJA	30
	0.64	JJA	12	-0.65	JJA	36
Needleleaf	0.60	JJA	60	-0.56	MAM	60
	0.58	JJA	48	-0.55	JJA	24
	0.55	JJA	36	-0.53	JJA	30
Eucalyptus	0.72	JJA	36	-0.77	JJA	24, 30, 36
	0.69	JJA	18	-0.76	JJA	18
	0.68	JJA, SON	48 (JJA), 18 (SON)	-0.65	JJA	12
Oak	0.60	JJA	3	-0.69	JJA	30
	0.59	JJA	60	-0.62	JJA	24
	0.52	JJA	2	-0.55	JJA	36
Annual Grass	0.66	DJF	4	-0.73	JJA	9, 10
	0.65	DJF	5	-0.72	JJA	8, 18
	0.64	DJF	9	-0.71	JJA	11, 12
Turfgrass	0.72	JJA	48	-0.68	JJA	36
	0.71	JJA, SON	36, 4	-0.64	JJA	18, 48
	0.69	SON	3	-0.61	JJA	30

The highest correlations between SPEI and NDVI were during summer (JJA) for most vegetation types, including broadleaf trees, needleleaf trees, Eucalyptus, oaks, and turfgrass. Annual grass NDVI had its highest correlations with SPEI during winter (DJF), which is indicative of its wintertime greening. Annual grass NDVI had significant correlations with SPEI spans ≤12 months exclusively, but this was not the case for other vegetation types. Most trees had their highest NDVI correlations with SPEI at spans of >12 months, likely due to their ability to use soil moisture at greater rooting depths, access stored carbon reserves, and delay phenological

494 expression in biomass (Kozlowski et al., 1991). The NDVI of evergreen oak trees was an
495 exception since it was poorly correlated with SPEI span overall. Turfgrass NDVI was most
496 strongly correlated with SPEI during fall (SON) and winter for SPEI spans <12 months, but had
497 many correlations during summer as well for spans >12 months.

498 In general, vegetation ΔLST was also most strongly correlated with SPEI spans during
499 summer as opposed to other seasons. Broadleaf, Eucalyptus, oaks, and turfgrass ΔLST only had
500 significant correlations ($p < 0.01$) with SPEI during summer (JJA) and during no other season.
501 Although it had many correlations during summer as well, needleleaf trees' ΔLST also had
502 significant correlations with SPEI during spring (MAM) at 48 and 60 month spans. In addition to
503 having its strongest correlations during the summer, annual grass was notable in that it was the
504 only vegetation type that had significant ΔLST correlations with SPEI during all four seasons.
505 However, while annual grass had the majority of its highest magnitude ΔLST correlations with
506 SPEI spans ≤12 months, all other vegetation types had their highest magnitude (i.e., most
507 negative) ΔLST correlations with SPEI spans >12 months. This may be due to shallow rooting
508 depths in annual grass as compared with trees, as well as the lack of irrigation in annual grass
509 compared to turfgrass leading to drying in surface soil. With prolonged interannual drought,
510 trees' modifications in leaf area may also affect their summer water use, leading to correlations
511 between SPEI and ΔLST at long time spans, in addition to any short term adjustments at a
512 seasonal scale.
513
514 3.4. EWT time series and comparison with NDVI

515 We calculated EWT from repeat AVIRIS imagery acquired during 2013-2015 to estimate
516 changes in canopy water content. For most vegetation types, EWT values decreased from spring
517 to fall, responding to continued summertime drawdown of available soil water (**Fig. 6**). Annual

grass only showed positive EWT values during spring, but annual grass EWT during summer and fall images were always equal to zero since it was senesced during these seasons. Trees generally had similar EWT values for similar seasons across years (e.g., comparing spring 2013 to spring 2015), and there was an apparent seasonal drawdown of available water from spring to fall corresponding to normal summer drought. However, oaks had anomalously high EWT during spring 2014 compared to 2013 or 2015. Turfgrass showed the greatest year over year declines in EWT during fall, with spring and summer declining from 2013 to 2015 as well; this suggests a reduction in irrigation watering as the interannual drought progressed.

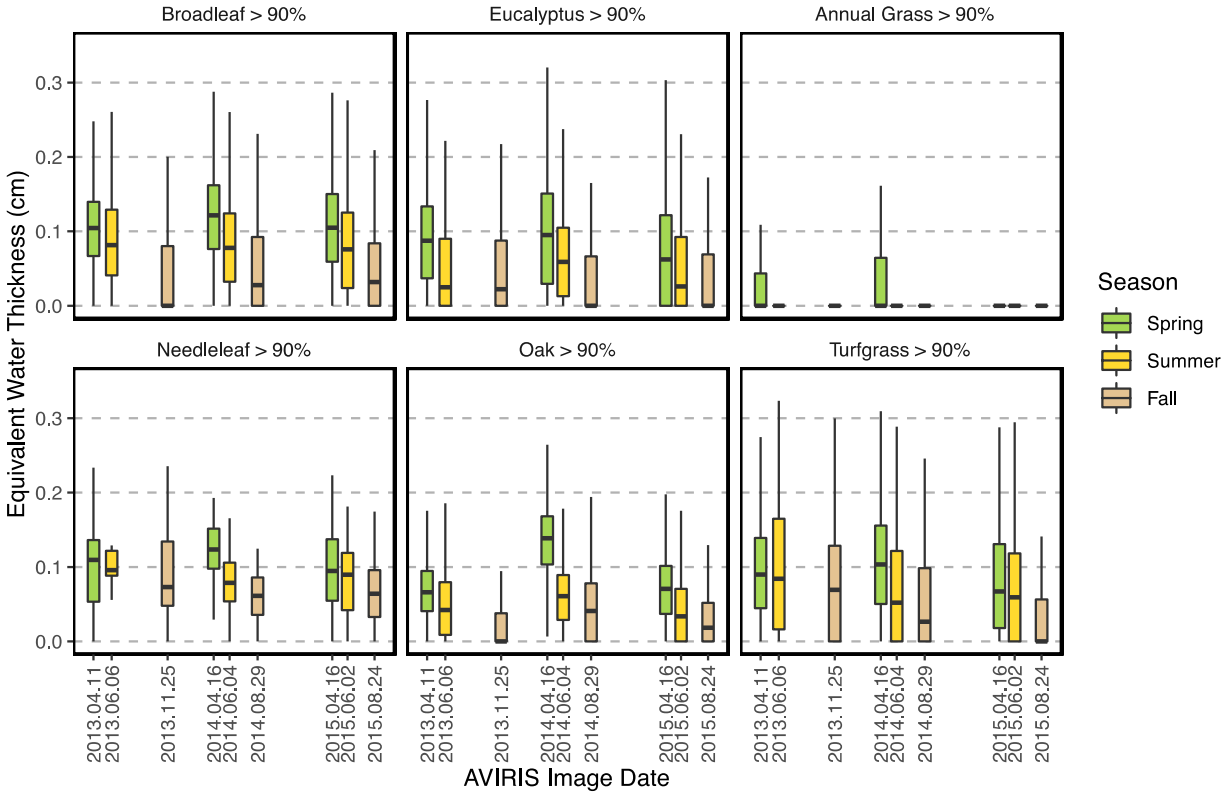

Fig. 6: Box plots of equivalent water thickness (EWT, cm) at AVIRIS image dates (2013-2015) for each vegetation cover type; x-axis is continuous to show the relative timing of image acquisitions (labels are Year.Month.Day) with acquisition seasons colored. Note broadleaf does

not include Eucalyptus or oak. Boxplot hinges extend to the 25th and 75th percentiles, whiskers extend to the farthest values within 1.5*interquartile range from each hinge, and outliers are omitted for clarity.

We compared changes in EWT to changes in simulated Landsat 5 TM NDVI from the AVIRIS time series. Box plots of NDVI by AVIRIS date, similar to **Fig. 6**, are shown in the supplemental material (**Fig. S3**). The overall relationship between EWT and NDVI was often nonlinear due to EWT approaching zero at moderate NDVI values, and EWT expanding to much higher values when NDVI did not change or was saturated at higher values (**Fig. 7**). At the same time, the relationships between median values of EWT and NDVI at each date were often linear (**Fig. 8**). The image acquired on 2013.11.25 was excluded from all regressions due to anomalously high NDVI, perhaps due highly off-nadir sun-sensor viewing geometry; in the regression for oaks, 2014.04.16 was also excluded due to anomalously high values of EWT. We were not able to create a regression for annual grass since its median EWT values were zero for all dates. Broadleaf, Eucalyptus, oaks, and turfgrass had slopes in the range of 1.09-1.25, while the slope for needleleaf trees was lower at 0.68. This indicates that needleleaf trees showed relatively little adjustment in NDVI relative to EWT compared to other vegetation types, which showed greater changes in NDVI with changes in EWT. Our calculated EWT approached zero even at moderate to high NDVI values (0.6-0.8) for the fall imagery for many vegetation types, suggesting a difference between overall vegetation greenness and water content. Despite lower NDVI values in Eucalyptus and needleleaf trees, EWT values showed seasonal adjustments similar to broadleaf trees, oaks, and turfgrass. Turfgrass NDVI was in a narrow range (0.64 - 0.70) for many dates; however, EWT showed wide variation in this same range of dates (0.026 - 0.100 cm).

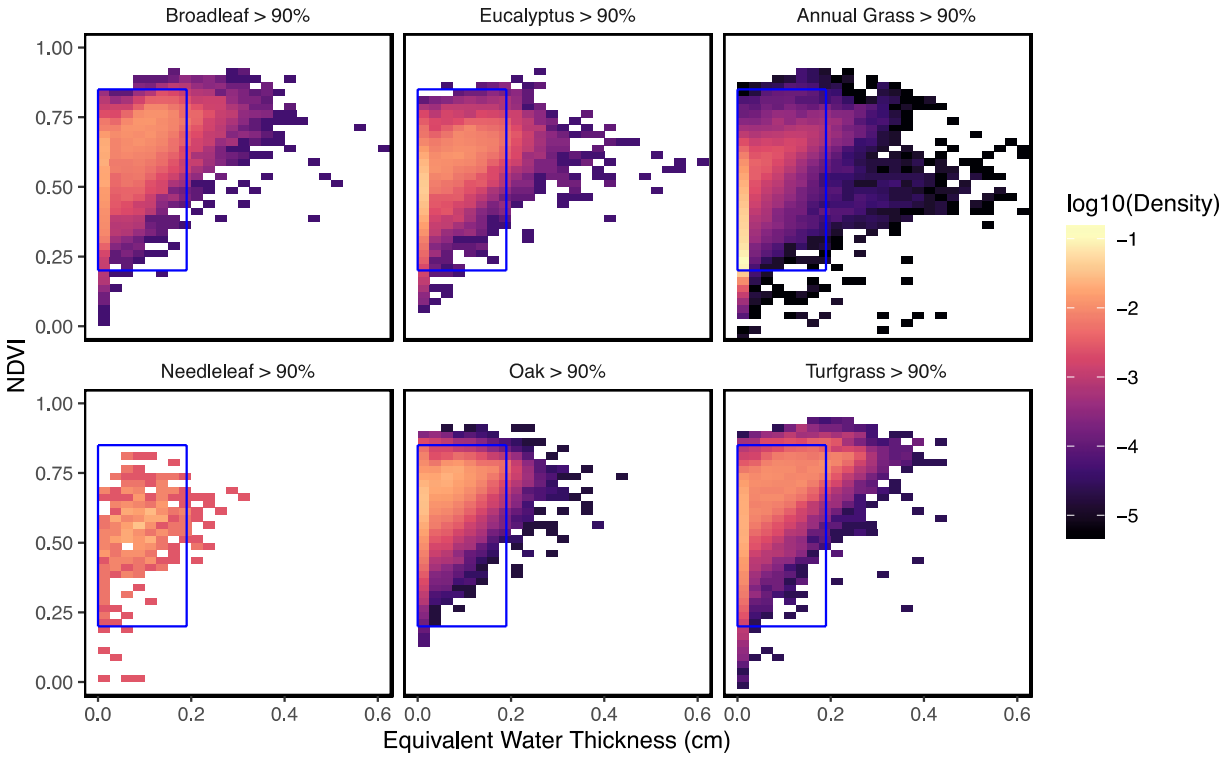

Fig. 7: Two-dimensional kernel density estimates of equivalent water thickness (EWT, x) vs. simulated Landsat 5 TM NDVI (y) for all AVIRIS flights for dominant vegetation cover types. Kernel density color bar has been $\log_{10}$-scaled for clarity. The blue box shows the range of **Fig. 8's** axes. Note values adjacent to the y-axis have EWT $\geq$ 0 cm since EWT cannot be negative, and few outliers EWT > 0.6 cm are not shown for clarity.

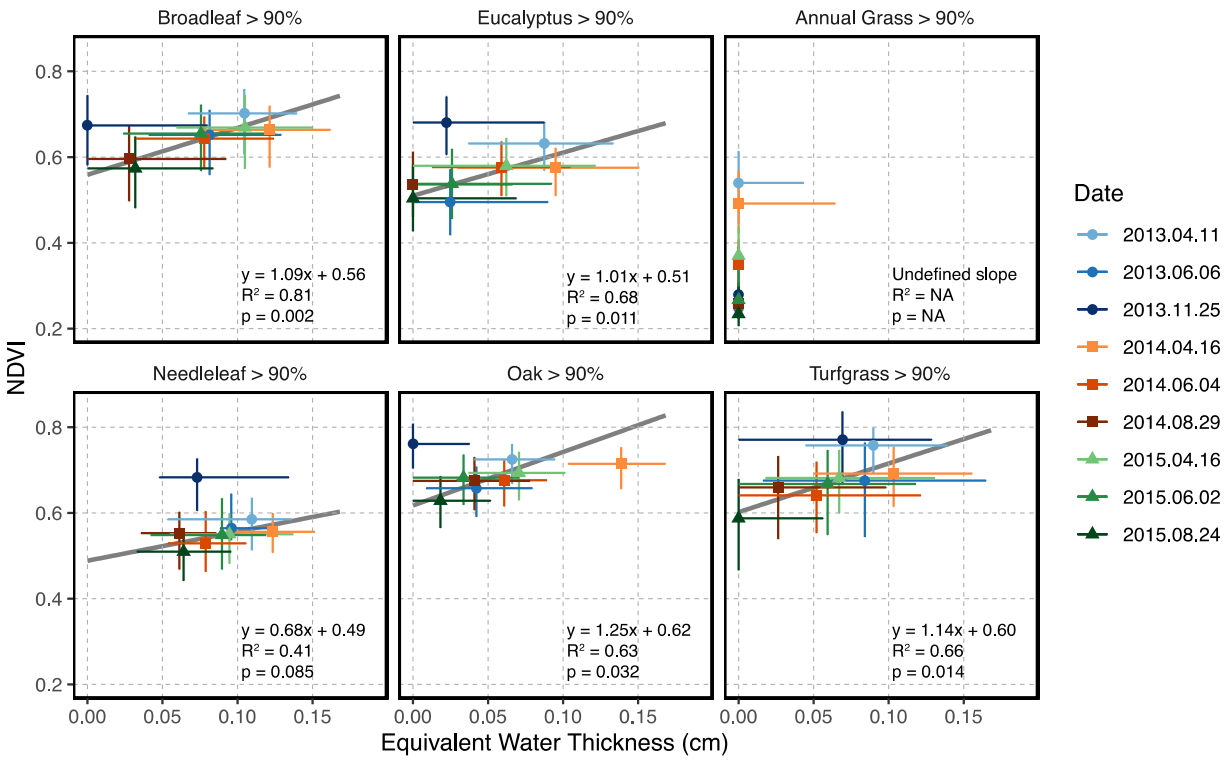

Fig. 8: Linear regressions of medians for equivalent water thickness (EWT, x) vs. simulated Landsat 5 TM NDVI (y) from all AVIRIS flights for all vegetation types. Colors and shapes indicate the date of AVIRIS flight (Year.Month.Day), and error bars are interquartile range. All linear regressions exclude 2013.11.25, and oak regression additionally excludes 2014.04.16.

We compared our estimates of EWT using broadleaf tree and shrub water mass data and spectra from Meerdink et al. (2016). We found that our estimates of leaf water mass, based on EWT, were overestimated and were not appropriate for individual leaves. However, the data did show a linear relationship (R^2 = 0.57; supplemental material, **Fig. S4**) and our mapped values from AVIRIS were within the ranges reported for other studies, albeit slightly low likely due to long-term drought (e.g., Roberts et al., 1997; Dennison et al., 2003; Sims and Gamon, 2003). EWT retrieved from spectra often overestimates leaf water estimates but underestimates total

canopy water estimates due to multiple near-infrared scattering in canopies (Roberts et al., 1997), and can vary depending on the spectral range used (e.g., Mobasheri and Fatemi, 2013). Additionally, EWT is most associated with the water content in all thin tissues rather than leaves or total canopy water content (Sims and Gamon, 2003).

4. Discussion

4.1. Overview

We evaluated the temporal effects of seasonal and interannual drought on urban trees and grasses, and compared vegetation response to drought based on three remote sensing variables related to different forms of plant function and characteristics (NDVI, ΔLST, and EWT). While most trees and turfgrass vegetation types in our Mediterranean-climate study area expressed drought response most prominently during seasonally-dry summer months, annual grass showed its greatest NDVI adjustments related to drought during winter, when precipitation would usually occur in non-drought years. Annual grass primarily showed its strongest correlations with adjustments in drought duration, using the SPEI (Vicente-Serrano et al., 2010; Abatzoglou et al., 2017), at time scales ≤12 months (i.e., seasonal droughts), while other vegetation types also showed strong correlations at time scales >12 months (i.e., interannual droughts). We compared the seasonal timing of changes in NDVI and ΔLST and found that these remote sensing variables were correlated for only some types of vegetation, often showing distinct changes in vegetation function separately related to greenness and evapotranspiration, respectively. We also demonstrated how, for vegetation types with higher leaf areas (i.e., trees and irrigated turfgrass), canopy water content from EWT showed a more pronounced response to seasonal drought than NDVI during the seasonal transition through spring, summer, and fall.

4.2. Vegetation cover of study area

We developed a land cover classification to be able to track different vegetation types through drought, using the larger Santa Barbara urbanized area to take advantage of greater vegetation area and larger tree stands that could be tracked with coarser spatial resolution Landsat and AVIRIS time series imagery. This expansion led to a greater proportion of vegetation and tree cover than might be expected in more densely populated cities nearby. Our study area (113 km^2) had 58% total vegetation cover (**Table 1**), which is higher than estimates for metropolitan Los Angeles, California (38.6% including senesced vegetation, McPherson et al., 2011; 31%, Wetherley et al., 2018), and our study area had 30% tree cover, which is also higher than Los Angeles (20.8%, McPherson et al., 2011; 20%; Wetherley et al., 2018). However, the vegetation (41%, this study) and tree cover (~24%; Alonzo et al., 2016) estimates for the denser Santa Barbara downtown area used by Alonzo et al. (2014; 2016) are lower and more similar to estimates for Los Angeles.

Although the coarser spatial resolutions for time series used here limited our ability to directly evaluate street trees and residential lawns, Miller et al. (2020) found that coast live oaks in smaller, more-urban patches and in larger, less-developed patches within the Santa Barbara downtown area both experienced severe response to the drought. While urban street tree drought response may differ from less densely developed areas due to potential irrigation inputs (Liang et al., 2017; Litvak et al., 2017) and increased thermal fluxes from impervious surfaces (Savi et al., 2015) for urban trees, Bijoor et al. (2012) found that some urban trees in metropolitan Los Angeles did not solely rely on irrigation for water and had remarkably similar water sources to non-urban riparian trees, which may enhance urban trees' ability to withstand drought by tapping deeper water sources.

4.3. Measured remote sensing variables and plant functional changes during drought

We assessed vegetation response to drought by using three different remote sensing variables in tandem: NDVI, ΔLST, and EWT. NDVI has formed the basis of many remote sensing studies vegetation response to drought (e.g., Sims et al., 2014), including those related to the SPEI (e.g., Vicente-Serrano et al., 2013; Rita et al., 2020). Similar to our results, other studies in similar California ecosystems have shown that evergreen trees and shrubs, such as oaks in this study (predominantly *Quercus agrifolia*), show relatively limited adjustments in NDVI throughout the year; in contrast, annual grasslands, like our annual grass class, show distinctly high NDVI values in the winter (Gamon et al., 1995). However, we found that large-canopied, evergreen Eucalyptus and needleleaf trees often showed increases in NDVI during winter (**Fig. 3**), which may be in part due to greening of the understory, but also due to the presence of cast shadows preferentially boosting near infrared reflectance relative to red at low solar elevation angles (Roberts et al., 1997). This effect was not as pronounced in smaller, dense-canopied oaks and broadleaf trees. Our results support the consensus that although many changes in vegetation canopies can be observed with greenness indices such as the NDVI, many adjustments related to plant function and structure, such as leaf surface temperature or water content, can occur without greenness changes (Asner et al., 2004; Zarco-Tejada et al., 2012; Sims et al., 2014).

In general, vegetation LST is reduced by evapotranspiration due to latent heat loss (Soer, 1980), which is tightly related to photosynthesis (Baldocchi et al., 2004), as well as canopy shadowing. We assessed vegetation LST as ΔLST, a differential from developed/impervious LST, to provide more stable estimates of the cooling potential of vegetation through time, taking account of variations in weather across the image acquisition dates. Estimates of ΔLST are likely related to soil water status and evaporation in addition to limited preceding plant growth. For example, since annual grass was senesced during all summers and would provide negligible

transpiration cooling in any summer, the reduced ΔLST during summer 2014 is likely related to limited soil water evaporation during an exceptional drought year. Overall, the ΔLST between vegetation and developed/impervious surfaces was minimized in winter but was larger and more variable in summer, similar to other studies (Liu and Weng, 2008; Haashemi et al., 2016; Meerdink et al., 2019b). While turfgrass and oaks in our study experienced changes in ΔLST, NDVI remained relatively stable. The other vegetation classes showed correlations between monthly values of ΔLST and NDVI, albeit weakly in the case of Eucalyptus (R = 0.25; **Fig. 4**). Although our ΔLST estimates likely may also be influenced by surface mixing due to resampling of the Landsat LST to 30 m (Malakar et al., 2018), we found that trees were often cooler than grass in spring and summer based on our mid-morning measurements from Landsat (e.g., for June 2013: broadleaf median ΔLST = -8.4 K, turfgrass median ΔLST = -7.0 K) which is consistent with other studies (Crum and Jenerette, 2017; Wetherley et al., 2018). However, Wetherley et al. (2018) also found that, across the Los Angeles basin, tree LST was consistently warmer than turfgrass LST when measured in the afternoon. Since LST varies diurnally, this variability can be better assessed with a sensor such as ECOSTRESS (Fisher et al., 2020) or with airborne acquisitions (e.g., Quattrochi and Ridd, 1998). We used LST measurements rather than air temperature, and air temperature can differ strongly from LST, especially beneath tree canopies (Shashua-Bar et al., 2009) and in areas near large tree stands (Ziter et al., 2019), although the magnitude of these effects can be highly variable (Manickathan et al., 2018). In general, tree canopy LST can often be significantly different from air temperature in this climate; this effect is more pronounced in summer and can also be highly variable by tree species (Meerdink et al., 2019b).

We found that EWT showed a more distinct seasonal response to drought than did NDVI for most vegetation types, as EWT was sensitive to vegetation drought responses in water content

672 and leaf area that were undetected by NDVI. This supports conclusions of previous studies
673 investigating seasonal changes in EWT (Roberts et al., 1997; Dennison et al., 2003; Ustin et al.,
674 2004) and comparing EWT to vegetation indices (e.g., Cheng et al., 2006). EWT showed a
675 nonlinear relationship with NDVI when evaluated at the pixel scale across all vegetation types
676 and dates, which is consistent with previous studies (e.g., Roberts et al., 2004). At the same time,
677 we also found that, for median values across dates, EWT showed a linear relationship to NDVI,
678 but the slopes of that relationship varied by vegetation type. Combined, these results suggest that
679 the relationship between EWT and NDVI is dependent on the type of vegetation canopy, and the
680 two variables are unlikely to be linearly related within the same acquisition or across many types
681 of vegetation. In particular, needleleaf trees had a lower slope (0.68) than other vegetation types
682 (1.01-1.14). Cheng et al. (2006) also found that EWT had a poorer linear relationship with NDVI
683 at conifer sites where NDVI appeared to saturate, as compared to grassland sites. We found that
684 median EWT was always zero for annual grass, which is likely due to our acquisitions having
685 occurred during a severe drought with low soil water outside of winter. Ustin et al. (2004) also
686 showed that annual grasses had EWT of zero for low soil water conditions. Our tree EWT
687 estimates were lower than in other studies for similar study areas (e.g., Dennison et al., 2003;
688 Ustin et al., 2004; Paz-Kagan and Asner, 2017). This may include error due to relatively large
689 pixels (18 m) covering mixed surfaces, understory vegetation senescence, and any potential
690 spatial misalignment between dates. However, these changes are also affected by extreme
691 drought conditions during the AVIRIS acquisitions (2013-2015). Overall, although EWT requires
692 measurements from imaging spectroscopy, our results suggest that future remote sensing studies
693 of vegetation drought response would likely benefit from the addition of EWT estimates through
694 time to supplement variables such as NDVI and ΔLST.
695

696 4.4. Seasonal and interannual drought expression in vegetation

697 We used the SPEI calculated at seasonal and interannual spans (Vicente-Serrano et al.,
698 2010; Abatzoglou et al., 2017) to examine the correlation of NDVI and ΔLST across different
699 vegetation types, following Vicente-Serrano et al. (2013) and Rita et al. (2020). This allowed us
700 to separate to impacts of seasonal variability in drought (expressed strongly in our annual grass
701 vegetation class) from interannual trends in drought (apparent in our tree and turfgrass classes).
702 The ability of trees to survive seasonal variability in drought matches our expectations from
703 previous work that trees in Mediterranean climates can access deeper water and therefore show
704 less sensitivity than grasses to seasonal variations in surface soil moisture, both in terms of
705 phenology and photosynthesis (e.g., Richardson et al., 2013; Sousa and Davis, 2020). For natural
706 landscapes near our study area, Coates et al. (2015) showed that trees are also often less sensitive
707 to drought than nearby chaparral vegetation.

708 By using both NDVI and ΔLST, we were able to show that these effects may not be
709 expressed at the same time of year for all urban tree and grass vegetation types. While
710 summertime reductions of soil-water during drought affected the ΔLST of all vegetation, it had
711 little effect on the NDVI of annual grasses due to their summertime senescence even in years of
712 normal rainfall. This implies that for our study area's climate, monitoring in winter is much more
713 important for annual grasses if using NDVI as a proxy for drought. At the same time, for trees,
714 summer is the most important time of year for to monitor drought based on NDVI, although
715 many trees show additional correlations during other seasons. Most vegetation cover types also
716 did not show correlations with SPEI at the 15 months span included in the calculations by
717 Abatzoglou et al. (2017), suggesting this span may be poor at capturing water status in this
718 climate, perhaps due to extreme interannual variability in rainfall during the drought time period.
719 Although we were not able to evaluate EWT as part of a correlation comparison with SPEI since

it had too few dates from AVIRIS as opposed to the NDVI and ΔLST collected from Landsat, we may have observed additional seasonal correlations with drought for otherwise evergreen vegetation (e.g., turfgrass, oaks).

Our study also showed different types of responses among tree vegetation types. We found that oaks and needleleaf trees had relatively few significant correlations with SPEI compared to other tree classes, suggesting different resource allocation strategies to weather drought (e.g., Dietze et al., 2014; Palacio al., 2018). Most of the oaks in our study region are primarily *Quercus agrifolia*, an evergreen species that avoids summer drought by shifting additional growth to the rainier winter months (Knops and Koenig, 1994). The needleleaf trees did not often occur in large stands and are likely more affected by mixing with impervious surfaces, which may have limited observable interannual variability at 30 m pixels. Common needleleaf species in our study area include *Pinus canariensis* and *Pinus pinea*, which are generally drought-tolerant species but were often affected during the 2012-2016 drought in this area (Miller et al., 2020).

The other trees classes in our study area included broadleaf trees and Eucalyptus, and these had more significant correlations with SPEI. Although there are wide varieties of both deciduous and evergreen broadleaf trees species in our study area (Alonzo et al., 2014; 2016), the thresholding for coarser Landsat time series often captured riparian areas, which often includes deciduous species such as *Platanus racemosa* and *Salix spp*. Other broadleaf species, including urban street trees, may behave differently (Bijoor et al., 2012), given that riparian areas experience drawdown of available water later in the year than in other locations (Sperry and Love, 2015). Our Eucalyptus class included many eucalypt species (e.g., *Eucalyptus sideroxylon*, *Corymbia citriodora*), but it consisted primarily of *Eucalyptus globulus*. This species is often considered to be drought-tolerant, but Mitchell et al. (2013) found that it has high water use

744 associated with its rapid growth rates. Specifically, *Eucalyptus globulus* keeps stomata open to
745 maintain lower turgor pressure, which is beneficial for continued growth during moderate
746 droughts but can cause swift hydraulic failure during more extreme water limitations due to the
747 tree's inability to downregulate its water use.

748 We used SPEI from a single location in downtown Santa Barbara to represent our full
749 study area because of its relatively small size (113 km^2) and due to the lack of scaling parameters
750 for local variability. We expect that with a much higher density of meteorological stations, our
751 results would have reflected more site-specific variability in the magnitude of drought impacts
752 and evapotranspiration (Savi et al., 2015; Crum and Jenerette, 2017; Litvak et al., 2017) due to
753 differences including soil type and topographic effects (e.g., Paz-Kagan and Asner, 2017), as well
754 as human management such as irrigation (Liang et al., 2017).

755 At the outset of our study, we had anticipated a more general disconnect of urban
756 vegetation from drought due to the availability of irrigation. For example, Buyantuyev and Wu
757 (2012) found that urban and riparian vegetation phenology in Phoenix, Arizona, were decoupled
758 from local climate variability, whereas natural desert vegetation was strongly regulated by the
759 preceding 3-5 months of precipitation and was negatively correlated with temperature. Turfgrass
760 in our study area can be assumed to be irrigated because it was green at the height of the long-
761 term drought in June 2014. Although our turfgrass samples also contained golf courses and
762 recreational areas due the restrictive nature of the coarse resolution imagery, in residential areas,
763 individual homeowners may have reduced lawn watering later in the drought due to water
764 conservation regulations (Council of the City of Santa Barbara, 2017) and public awareness
765 campaigns (McCumber, 2017). Only in the spring did our results from turfgrass support the
766 notion of climatological disconnect from drought. Turfgrass NDVI showed correlation with SPEI
767 spans of <12 months during fall and winter, and with SPEI spans >12 months for winter,

768 summer, and fall. This indicates that even typically irrigated urban vegetation is not fully
769 insulated from seasonal drought at the city scale, and it is consistent with other studies showing
770 the impacts of interannual drought on turfgrass in metropolitan California (Quesnel et al., 2019;
771 Miller et al., 2020).
772
773 **5. Conclusions**
774 Different functional types of urban vegetation can show a diverse array of responses to
775 drought related to different plant canopy characteristics and seasonal timing. In this study, we
776 evaluated both the magnitude and seasonal timing of spectral responses among urban trees
777 (broadleaf, needleleaf, Eucalyptus, and oak) and grasses (annual grass, turfgrass) to seasonal and
778 interannual drought duration via the SPEI, addressing three main goals.
779 First, we compared adjustments in NDVI and ΔLST (from Landsat) and EWT (from
780 AVIRIS) among different vegetation types during the study time period. Broadleaf trees,
781 Eucalyptus trees, and annual grass had distinct seasonal patterns in NDVI, while needleleaf trees,
782 evergreen oaks, and turfgrass showed comparatively less seasonal change in NDVI. Seasonal
783 patterns in ΔLST were largely similar among all vegetation types, with the most substantial
784 difference between vegetation and developed/impervious LST observed during the summer.
785 EWT showed seasonal reductions of water content for all vegetation types except for annual
786 grass, which was primarily senesced in nearly all the 2013-2015 AVIRIS acquisitions due to
787 long-term drought.
788 Second, to evaluate the seasonal variation of plant response to drought duration across
789 different vegetation types, we examined the correlation of changes in NDVI and ΔLST to
790 changes in SPEI calculated at a range of time spans. This correlation allowed us to both assess
791 the length of drought most associated with vegetation response and determine the season that this

response was most apparent. Generally, NDVI was positively correlated with SPEI, and ΔLST was negatively correlated with SPEI. In most of the vegetation types we studied, NDVI had the strongest correlations (i.e., most positive) with SPEI during summer, except for annual grass, which had its strongest NDVI correlations with SPEI during winter. Similarly, ΔLST correlations with SPEI were strongest (i.e., most negative) for all vegetation types during summer. Annual grass had nearly all its greatest correlations at SPEI spans of ≤12 months for both NDVI and ΔLST, indicating its primary response to seasonal variation in water availability. In contrast, although they showed seasonal response as well, trees and turfgrass had many correlations with SPEI spans >12 months for both NDVI and ΔLST, indicating a significant response to interannual drought and reflecting trees' ability access deeper water and utilize stored resources that are unavailable to annual grasses.

Lastly, using repeat AVIRIS acquisitions, we compared seasonal and interannual changes in EWT to changes in simulated Landsat NDVI to investigate the complementary information provided by this imaging spectroscopy measurement for our study period. These results suggest that EWT and NDVI provide different information regarding canopy condition, and cannot be directly regressed across many types of vegetation. For trees and turfgrass, EWT showed seasonal changes from spring to fall that was not as readily apparent in NDVI. EWT overall had a nonlinear response to NDVI when combining all available pixels across all dates for each vegetation type; however, although EWT generally had linear relationships with NDVI when comparing median values across dates, the slopes and intercepts of these relationships varied between different vegetation types. These results support past research studies that suggest EWT can be a valuable addition to remote sensing studies of vegetation canopy condition and drought, namely by often showing further adjustments in canopy water content and leaf area in canopies where NDVI may be relatively invariant, and this is an example of an important use-case of a

potential spaceborne imaging spectrometer such as the NASA Surface Biology and Geology (SBG) mission.

Our results provide insights into the sensitivity of different vegetation types to drought at a range of temporal scales, and demonstrate how jointly using complementary remote sensing variables (NDVI, ΔLST, EWT) can improve assessment of drought-induced change in vegetation canopies. With many cities likely to undergo changing climate conditions, annual maps at a single time of year are unlikely to be sufficient to evaluate the breadth of potential impacts to ecosystem services in urban vegetation, and many natural areas may experience similar effects in regards to drought and climate. As a consequence, the techniques used in this study are by no means unique to urban areas and could be broadly applied to natural ecosystems to investigate vegetation response to drought.

Acknowledgments

This study was supported by a NASA Earth and Space Science Fellowship (80NSSC18K1325). Special thanks to Erin Wetherley, Christopher Heckman, S. Lucille Blakeley, Lauren Smyth, and James Allen for data availability, methodological comments, and/or editorial suggestions.

References

Abatzoglou, J.T., McEvoy, D.J., Redmond, K.T., 2017. The West Wide Drought Tracker: Drought Monitoring at Fine Spatial Scales. Bull. Am. Meteorol. Soc. 98, 1815–1820. https://doi.org/10.1175/bams-d-16-0193.1

Alonzo, M., Bookhagen, B., Roberts, D.A., 2014. Urban tree species mapping using hyperspectral and lidar data fusion. Remote Sens. Environ. 148, 70–83. https://doi.org/10.1016/j.rse.2014.03.018

Alonzo, M., McFadden, J.P., Nowak, D.J., Roberts, D.A., 2016. Mapping urban forest structure and function using hyperspectral imagery and lidar data. Urban For. Urban Green. 17, 135–147. https://doi.org/10.1016/j.ufug.2016.04.003

Asner, G.P., Nepstad, D., Cardinot, G., Ray, D., 2004. Drought stress and carbon uptake in an Amazon forest measured with spaceborne imaging spectroscopy. Proc. Natl. Acad. Sci. U. S. A. 101, 6039–6044. https://doi.org/10.1073/pnas.0400168101

Asner, G.P., Brodrick, P.G., Anderson, C.B., Vaughn, N., Knapp, D.E., Martin, R.E., 2016. Progressive forest canopy water loss during the 2012–2015 California drought. Proc. Natl. Acad. Sci. 113, 201523397. https://doi.org/10.1073/pnas.1523397113

Avolio, M., Pataki, D.E., Jenerette, G.D., Pincetl, S., Clarke, L.W., Cavender- Bares, J., Gillespie, T.W., Hobbie, S.E., Larson, K.L., McCarthy, H.R., Trammell, T.L.E., 2020. Urban plant diversity in Los Angeles, California: Species and functional type turnover in cultivated landscapes. Plants, People, Planet 2, 144–156. https://doi.org/10.1002/ppp3.10067

Baldocchi, D.D., Xu, L.K., Kiang, N., 2004. How plant functional-type, weather, seasonal drought, and soil physical properties alter water and energy fluxes of an oak-grass savanna and an annual grassland. Agric. For. Meteorol. 123, 13–39.

Barbeta, A., Ogaya, R., Peñuelas, J., 2013. Dampening effects of long-term experimental drought on growth and mortality rates of a Holm oak forest. Glob. Chang. Biol. 19, 3133–3144. https://doi.org/10.1111/gcb.12269

Belgiu, M., Drăguţ, L., 2016. Random forest in remote sensing: A review of applications and future directions. ISPRS J. Photogramm. Remote Sens. 114, 24–31. https://doi.org/10.1016/j.isprsjprs.2016.01.011

Bijoor, N.S., McCarthy, H.R., Zhang, D., Pataki, D.E., 2012. Water sources of urban trees in the Los Angeles metropolitan area. Urban Ecosyst. 15, 195–214. https://doi.org/10.1007/s11252-011-0196-1

Bréda, N., Huc, R., Granier, A., Dreyer, E., 2006. Temperate forest trees and stands under severe drought: a review of ecophysiological responses, adaptation processes and long-term consequences. Ann. For. Sci. 63, 625–644. https://doi.org/10.1051/forest:2006042

Breiman, L., 2001. Random Forests. Mach. Learn. 45, 5–32. https://doi.org/10.1023/A:1010933404324

Buyantuyev, A., Wu, J., 2012. Urbanization diversifies land surface phenology in arid environments: Interactions among vegetation, climatic variation, and land use pattern in the Phoenix metropolitan region, USA. Landsc. Urban Plan. 105, 149–159. https://doi.org/10.1016/j.landurbplan.2011.12.013

Byrd, R.H., Lu, P., Nocedal, J., Zhu, C., 1995. A Limited Memory Algorithm for Bound Constrained Optimization. SIAM J. Sci. Comput. 16, 1190–1208. https://doi.org/10.1137/0916069

Cadenasso, M.L., Pickett, S.T.A., Schwarz, K., 2007. Spatial heterogeneity in urban ecosystems: reconceptualizing land cover and a framework for classification. Front. Ecol. Environ. 5, 80–88. https://doi.org/10.1890/1540-9295(2007)5[80:SHIUER]2.0.CO;2

881 Cheng, Y. Ben, Zarco-Tejada, P.J., Riaño, D., Rueda, C.A., Ustin, S.L., 2006. Estimating
882 vegetation water content with hyperspectral data for different canopy scenarios:
883 Relationships between AVIRIS and MODIS indexes. Remote Sens. Environ. 105, 354–366.
884 https://doi.org/10.1016/j.rse.2006.07.005
885 Clark, R.N., Roush, T.L., 1984. Reflectance spectroscopy: Quantitative analysis techniques for
886 remote sensing applications. J. Geophys. Res. Solid Earth 89, 6329–6340.
887 https://doi.org/10.1029/JB089iB07p06329
888 Coates, A.R., Dennison, P.E., Roberts, D.A., Roth, K.L., 2015. Monitoring the impacts of severe
889 drought on southern California chaparral species using hyperspectral and thermal infrared
890 imagery. Remote Sens. 7, 14276–14291. https://doi.org/10.3390/rs71114276
891 Cook, M., Schott, J.R., Mandel, J., Raqueno, N., 2014. Development of an operational calibration
892 methodology for the Landsat thermal data archive and initial testing of the atmospheric
893 compensation component of a land surface temperature (LST) product from the archive.
894 Remote Sens. 6, 11244–11266. https://doi.org/10.3390/rs61111244
895 Council of the City of Santa Barbara, 2017. Resolution No. 17-017. Santa Barbara, California.
896 Crum, S.M., Darrel Jenerette, G., 2017. Microclimate variation among urban land covers: The
897 importance of vertical and horizontal structure in air and land surface temperature
898 relationships. J. Appl. Meteorol. Climatol. 56, 2531–2543. https://doi.org/10.1175/JAMC-D-
899 17-0054.1
900 Dennison, P.E., Roberts, D.A., Thorgusen, S.R., Regelbrugge, J.C., Weise, D., Lee, C., 2003.
901 Modeling seasonal changes in live fuel moisture and equivalent water thickness using a
902 cumulative water balance index. Remote Sens. Environ. 88, 442–452.
903 https://doi.org/10.1016/j.rse.2003.08.015

Dietze, M.C., Sala, A., Carbone, M.S., Czimczik, C.I., Mantooth, J.A., Richardson, A.D., Vargas, R., 2014. Nonstructural Carbon in Woody Plants. Annu. Rev. Plant Biol. 65, 667–687. https://doi.org/10.1146/annurev-arplant-050213-040054

Diffenbaugh, N.S., Swain, D.L., Touma, D., 2015. Anthropogenic warming has increased drought risk in California. Proc. Natl. Acad. Sci. 112, 3931–3936. https://doi.org/10.1073/pnas.1422385112

Dong, C., MacDonald, G.M., Willis, K., Gillespie, T.W., Okin, G.S., Williams, A.P., 2019. Vegetation Responses to 2012–2016 Drought in Northern and Southern California. Geophys. Res. Lett. 46, 3810–3821. https://doi.org/10.1029/2019GL082137

Dwyer, J.L., Roy, D.P., Sauer, B., Jenkerson, C.B., Zhang, H.K., Lymburner, L., 2018. Analysis ready data: Enabling analysis of the landsat archive. Remote Sens. 10, 1–19. https://doi.org/10.3390/rs10091363

Fisher, J.B., Lee, B., Purdy, A.J., Halverson, G.H., Dohlen, M.B., Cawse- Nicholson, K., Wang, A., Anderson, R.G., Aragon, B., Arain, M.A., Baldocchi, D.D., Baker, J.M., Barral, H., Bernacchi, C.J., Bernhofer, C., Biraud, S.C., Bohrer, G., Brunsell, N., Cappelaere, B., Castro- Contreras, S., Chun, J., Conrad, B.J., Cremonese, E., Demarty, J., Desai, A.R., De Ligne, A., Foltýnová, L., Goulden, M.L., Griffis, T.J., Grünwald, T., Johnson, M.S., Kang, M., Kelbe, D., Kowalska, N., Lim, J., Maïnassara, I., McCabe, M.F., Missik, J.E.C., Mohanty, B.P., Moore, C.E., Morillas, L., Morrison, R., Munger, J.W., Posse, G., Richardson, A.D., Russell, E.S., Ryu, Y., Sanchez- Azofeifa, A., Schmidt, M., Schwartz, E., Sharp, I., Šigut, L., Tang, Y., Hulley, G., Anderson, M., Hain, C., French, A., Wood, E., Hook, S., 2020. ECOSTRESS: NASA's Next Generation Mission to Measure Evapotranspiration From the International Space Station. Water Resour. Res. 56, 1–20. https://doi.org/10.1029/2019WR026058

928 Gamon, J.A., Field, C.B., Goulden, M.L., Griffin, K.L., Anne, E., Joel, G., Peñuelas, J.,
929 Valentini, R., 1995. Relationships Between NDVI, Canopy Structure, and Photosynthesis in
930 Three Californian Vegetation Types. Ecol. Appl. 5, 28–41.
931 Gouveia, C.M., Trigo, R.M., Beguería, S., Vicente-Serrano, S.M., 2017. Drought impacts on
932 vegetation activity in the Mediterranean region: An assessment using remote sensing data
933 and multi-scale drought indicators. Glob. Planet. Change 151, 15–27.
934 https://doi.org/10.1016/j.gloplacha.2016.06.011
935 Green, R.O., Conel, J.E., Roberts, D.A., 1993. Estimation of aerosol optical depth, pressure
936 elevation, water vapor, and calculation of apparent surface reflectance from radiance
937 measured by the airborne visible/infrared imaging spectrometer (AVIRIS) using a radiative
938 transfer code. Imaging Spectrom. Terr. Environ. 1937, 2. https://doi.org/10.1117/12.157054
939 Green, R.O., Eastwood, M.L., Sarture, C.M., Chrien, T.G., Aronsson, M., Chippendale, B.J.,
940 Faust, J.A., Pavri, B.E., Chovit, C.J., Solis, M., Olah, M.R., Williams, O., 1998. Imaging
941 spectroscopy and the Airborne Visible/Infrared Imaging Spectrometer (AVIRIS). Remote
942 Sens. Environ. 65, 227–248. https://doi.org/10.1016/S0034-4257(98)00064-9
943 Haashemi, S., Weng, Q., Darvishi, A., Alavipanah, S.K., 2016. Seasonal variations of the surface
944 urban heat Island in a semi-arid city. Remote Sens. 8. https://doi.org/10.3390/rs8040352
945 Hamlin, L., Green, R.O., Mouroulis, P., Eastwood, M., Wilson, D., Dudik, M., Paine, C., 2011.
946 Imaging spectrometer science measurements for terrestrial ecology: AVIRIS and new
947 developments. IEEE Aerosp. Conf. Proc. 1–7. https://doi.org/10.1109/AERO.2011.5747395
948 Hanson, P.J., Weltzin, J.F., 2000. Drought disturbance from climate change: Response of United
949 States forests. Sci. Total Environ. 262, 205–220. https://doi.org/10.1016/S0048-
950 9697(00)00523-4

951 Herold, M., Roberts, D.A., Gardner, M.E., Dennison, P.E., 2004. Spectrometry for urban area
952 remote sensing - Development and analysis of a spectral library from 350 to 2400 nm.
953 Remote Sens. Environ. 91, 304–319. https://doi.org/10.1016/j.rse.2004.02.013
954 Hoffman, J.S., Shandas, V., Pendleton, N., 2020. The Effects of Historical Housing Policies on
955 Resident Urban Areas. Climate 8, 1–15.
956 Ivits, E., Horion, S., Fensholt, R., Cherlet, M., 2014. Drought footprint on European ecosystems
957 between 1999 and 2010 assessed by remotely sensed vegetation phenology and productivity.
958 Glob. Chang. Biol. 20, 581–593. https://doi.org/10.1111/gcb.12393
959 Kean, J.W., Staley, D.M., Lancaster, J.T., Rengers, F.K., Swanson, B.J., Coe, J.A., Hernandez,
960 J.L., Sigman, A.J., Allstadt, K.E., Lindsay, D.N., 2019. Inundation, flow dynamics, and
961 damage in the 9 January 2018 Montecito debris-flow event, California, USA: Opportunities
962 and challenges for post-wildfire risk assessment. Geosphere 15, 1140–1163.
963 https://doi.org/10.1130/GES02048.1
964 Knops, J.M.H., Koenig, W.D., 1994. Water use strategies of five sympatric species of Quercus in
965 central coastal California. Madrono 41, 290–301.
966 Kozlowksi, T.T., Kramer, P.J., Pallardy, S.G., 1991. The Physiological Ecology of Woody
967 Plants. Elsevier. https://doi.org/10.1016/C2009-0-02706-8
968 Lee, C.M., Cable, M.L., Hook, S.J., Green, R.O., Ustin, S.L., Mandl, D.J., Middleton, E.M.,
969 2015. An introduction to the NASA Hyperspectral InfraRed Imager (HyspIRI) mission and
970 preparatory activities. Remote Sens. Environ. 167, 6–19.
971 https://doi.org/10.1016/j.rse.2015.06.012
972 Leuzinger, S., Vogt, R., Körner, C., 2010. Tree surface temperature in an urban environment.
973 Agric. For. Meteorol. 150, 56–62. https://doi.org/10.1016/j.agrformet.2009.08.006

974 Liang, L.L., Anderson, R.G., Shiflett, S.A., Jenerette, G.D., 2017. Urban outdoor water use and
975 response to drought assessed through mobile energy balance and vegetation greenness
976 measurements. Environ. Res. Lett. 12. https://doi.org/10.1088/1748-9326/aa7b21
977 Litvak, E., Manago, K.F., Hogue, T.S., Pataki, D.E., 2017. Evapotranspiration of urban
978 landscapes in Los Angeles, California at the municipal scale. Water Resour. Res. 53, 4236–
979 4252. https://doi.org/10.1002/2016WR020254
980 Liu, H., Weng, Q., 2008. Seasonal variations in the relationship between landscape pattern and
981 land surface temperature in Indianapolis, USA. Environ. Monit. Assess. 144, 199–219.
982 https://doi.org/10.1007/s10661-007-9979-5
983 Lund, J., Medellin-Azuara, J., Durand, J., Stone, K., 2018. Lessons from California's 2012–2016
984 Drought. J. Water Resour. Plan. Manag. 144, 04018067.
985 https://doi.org/10.1061/(asce)wr.1943-5452.0000984
986 Malakar, N.K., Hulley, G.C., Hook, S.J., Laraby, K., Cook, M., Schott, J.R., 2018. An
987 Operational Land Surface Temperature Product for Landsat Thermal Data: Methodology
988 and Validation. IEEE Trans. Geosci. Remote Sens. 56, 5717–5735.
989 https://doi.org/10.1109/TGRS.2018.2824828
990 Manickathan, L., Defraeye, T., Allegrini, J., Derome, D., Carmeliet, J., 2018. Parametric study of
991 the influence of environmental factors and tree properties on the transpirative cooling effect
992 of trees. Agric. For. Meteorol. 248, 259–274.
993 https://doi.org/10.1016/j.agrformet.2017.10.014
994 McCumber, A., 2017. Building "natural" beauty: Drought and the shifting aesthetics of nature in
995 Santa Barbara, California. Nat. Cult. 12, 246–262. https://doi.org/10.3167/nc.2017.120303
996 McPherson, E.G., Simpson, J.R., Xiao, Q.F., Wu, C.X., 2011. Million trees Los Angeles canopy
997 cover and benefit assessment. Landsc. Urban Plan. 99, 40–50.

McPherson, E.G., Berry, A.M., van Doorn, N.S., 2018. Performance testing to identify climate-ready trees. Urban For. Urban Green. 29, 28–39. https://doi.org/10.1016/j.ufug.2017.09.003

Meerdink, S.K., Roberts, D.A., King, J.Y., Roth, K.L., Dennison, P.E., Amaral, C.H., Hook, S.J., 2016. Linking seasonal foliar traits to VSWIR-TIR spectroscopy across California ecosystems. Remote Sens. Environ. 186, 322–338. https://doi.org/10.1016/j.rse.2016.08.003

Meerdink, S.K., Roberts, D.A., Roth, K.L., King, J.Y., Gader, P.D., Koltunov, A., 2019a. Classifying California plant species temporally using airborne hyperspectral imagery. Remote Sens. Environ. 232, 111308. https://doi.org/10.1016/j.rse.2019.111308

Meerdink, S., Roberts, D.A., Hulley, G., Pisek, J., Raabe, K., King, J., Hook, S.J., 2019b. Plant species' spectral emissivity and temperature using the Hyperspectral Thermal Emission Spectrometer (HyTES) sensor. Remote Sens. Environ. 224, 421–435. https://doi.org/10.1016/j.rse.2019.02.009

Miller, D.L., Alonzo, M., Roberts, D.A., Tague, C.L., McFadden, J.P., 2020. Drought response of urban trees and turfgrass using airborne imaging spectroscopy. Remote Sens. Environ. 240, 111646. https://doi.org/10.1016/j.rse.2020.111646

Mitchell, P.J., O'Grady, A.P., Tissue, D.T., White, D.A., Ottenschlaeger, M.L., Pinkard, E.A., 2013. Drought response strategies define the relative contributions of hydraulic dysfunction and carbohydrate depletion during tree mortality. New Phytol. 197, 862–872. https://doi.org/10.1111/nph.12064

Mobasheri, M.R., Fatemi, S.B., 2013. Leaf Equivalent Water Thickness assessment using reflectance at optimum wavelengths. Theor. Exp. Plant Physiol. 25, 196–202. https://doi.org/10.1590/S2197-00252013005000001

National Centers for Environmental Information, 2019. Summary of Monthly Normals 1981-2010: Santa Barbara Municipal Airport, CA US USW00023190. Asheville, North Carolina.

1022 Norton, B.A., Coutts, A.M., Livesley, S.J., Harris, R.J., Hunter, A.M., Williams, N.S.G., 2015.
1023 Planning for cooler cities: A framework to prioritise green infrastructure to mitigate high
1024 temperatures in urban landscapes. Landsc. Urban Plan. 134, 127–138.
1025 https://doi.org/10.1016/j.landurbplan.2014.10.018
1026 Okin, G.S., Dong, C., Willis, K.S., Gillespie, T.W., MacDonald, G.M., 2018. The Impact of
1027 Drought on Native Southern California Vegetation: Remote Sensing Analysis Using
1028 MODIS-Derived Time Series. J. Geophys. Res. Biogeosciences 123, 1927–1939.
1029 https://doi.org/10.1029/2018JG004485
1030 Otkin, J.A., Svoboda, M., Hunt, E.D., Ford, T.W., Anderson, M.C., Hain, C., Basara, J.B., 2018.
1031 Flash Droughts: A Review and Assessment of the Challenges Imposed by Rapid-Onset
1032 Droughts in the United States. Bull. Am. Meteorol. Soc. 99, 911–919.
1033 https://doi.org/10.1175/BAMS-D-17-0149.1
1034 Palacio, S., Camarero, J.J., Maestro, M., Alla, A.Q., Lahoz, E., Montserrat-Martí, G., 2018. Are
1035 storage and tree growth related? Seasonal nutrient and carbohydrate dynamics in evergreen
1036 and deciduous Mediterranean oaks. Trees 32, 777–790. https://doi.org/10.1007/s00468-018-
1037 1671-6
1038 Palazzo, J., Liu, O.R., Stillinger, T., Song, R., Wang, Y., Hiroyasu, E.H.T., Zenteno, J.,
1039 Anderson, S., Tague, C., 2017. Urban responses to restrictive conservation policy during
1040 drought. Water Resour. Res. 53, 4459–4475. https://doi.org/10.1002/2016WR020136
1041 Paz-Kagan, T., Asner, G.P., 2017. Drivers of woody canopy water content responses to drought
1042 in a Mediterranean-type ecosystem. Ecol. Appl. 27, 2220–2233.
1043 https://doi.org/10.1002/eap.1603

1044 Pincetl, S., Gillespie, T.W., Pataki, D.E., Porse, E., Jia, S., Kidera, E., Nobles, N., Rodriguez, J.,
1045 Choi, D., 2019. Evaluating the effects of turf-replacement programs in Los Angeles. Landsc.
1046 Urban Plan. 185, 210–221. https://doi.org/10.1016/j.landurbplan.2019.01.011
1047 Quattrochi, D.A., Ridd, M.K., 1998. Analysis of vegetation within a semi-arid urban environment
1048 using high spatial resolution airborne thermal infrared remote sensing data. Atmos. Environ.
1049 32, 19–33. https://doi.org/10.1016/S1352-2310(97)00179-9
1050 Quesnel, K.J., Ajami, N., Marx, A., 2019. Shifting landscapes: decoupled urban irrigation and
1051 greenness patterns during severe drought. Environ. Res. Lett. 14, 064012.
1052 https://doi.org/10.1088/1748-9326/ab20d4
1053 Richardson, A.D., Keenan, T.F., Migliavacca, M., Ryu, Y., Sonnentag, O., Toomey, M., 2013.
1054 Climate change, phenology, and phenological control of vegetation feedbacks to the climate
1055 system. Agric. For. Meteorol. 169, 156–173.
1056 https://doi.org/10.1016/j.agrformet.2012.09.012
1057 Rita, A., Camarero, J.J., Nolè, A., Borghetti, M., Brunetti, M., Pergola, N., Serio, C.,
1058 Vicente- Serrano, S.M., Tramutoli, V., Ripullone, F., 2020. The impact of drought spells on
1059 forests depends on site conditions: The case of 2017 summer heat wave in southern Europe.
1060 Glob. Chang. Biol. 26, 851–863. https://doi.org/10.1111/gcb.14825
1061 Roberts, D.A., Green, R.O., Adams, J.B., 1997. Temporal and spatial patterns in vegetation and
1062 atmospheric properties from AVIRIS. Remote Sens. Environ. 62, 223–240.
1063 https://doi.org/10.1016/S0034-4257(97)00092-8
1064 Roberts, D.A., Ustin, S.L., Ogunjemiyo, S., Greenberg, J., Dobrowski, S.Z., Chen, J., Hinckley,
1065 T.M., 2004. Spectral and Structural Measures of Northwest Forest Vegetation at Leaf to
1066 Landscape Scales. Ecosystems 7, 545–562. https://doi.org/10.1007/s10021-004-0144-5

1067 Rouse, J.W., Haas, R.H., Schell, J.A., Deering, D.W., 1973. Monitoring vegetation systems in the
1068 great plains with ERTS, in: Third ETS Symposium, Vol. 1. NASA SP-351, NASA,
1069 Washington, DC, pp. 309–317.
1070 Roy, D.P., Kovalskyy, V., Zhang, H.K., Vermote, E.F., Yan, L., Kumar, S.S., Egorov, A., 2016.
1071 Characterization of Landsat-7 to Landsat-8 reflective wavelength and normalized difference
1072 vegetation index continuity. Remote Sens. Environ. 185, 57–70.
1073 https://doi.org/10.1016/j.rse.2015.12.024
1074 Savi, T., Bertuzzi, S., Branca, S., Tretiach, M., Nardini, A., 2015. Drought-induced xylem
1075 cavitation and hydraulic deterioration: Risk factors for urban trees under climate change?
1076 New Phytol. 205, 1106–1116. https://doi.org/10.1111/nph.13112
1077 Schlesinger, W.H., Dietze, M.C., Jackson, R.B., Phillips, R.P., Rhoades, C.C., Rustad, L.E.,
1078 Vose, J.M., 2016. Forest biogeochemistry in response to drought. Glob. Chang. Biol. 22,
1079 2318–2328. https://doi.org/10.1111/gcb.13105
1080 Serrano, L., Ustin, S.L., Roberts, D.A., Gamon, J.A., Peñuelas, J., 2000. Deriving water content
1081 of chaparral vegetation from AVIRIS data. Remote Sens. Environ. 74, 570–581.
1082 https://doi.org/10.1016/S0034-4257(00)00147-4
1083 Shashua-Bar, L., Pearlmutter, D., Erell, E., 2009. The cooling efficiency of urban landscape
1084 strategies in a hot dry climate. Landsc. Urban Plan. 92, 179–186.
1085 https://doi.org/10.1016/j.landurbplan.2009.04.005
1086 Shivers, S.W., Roberts, D.A., McFadden, J.P., Tague, C., 2018. Using Imaging Spectrometry to
1087 Study Changes in Crop Area in California's Central Valley during Drought. Remote Sens.
1088 10, 1–30. https://doi.org/10.3390/rs10101556

1089 Sims, D.A., Brzostek, E.R., Rahman, A.F., Dragoni, D., Phillips, R.P., 2014. An improved
1090 approach for remotely sensing water stress impacts on forest C uptake. Glob. Chang. Biol.
1091 20, 2856–2866. https://doi.org/10.1111/gcb.12537
1092 Sims, D.A., Gamon, J.A., 2003. Estimation of vegetation water content and photosynthetic tissue
1093 area from spectral reflectance: A comparison of indices based on liquid water and
1094 chlorophyll absorption features. Remote Sens. Environ. 84, 526–537.
1095 https://doi.org/10.1016/S0034-4257(02)00151-7
1096 Soer, G.J.R., 1980. Estimation of regional evapotranspiration and soil moisture conditions using
1097 remotely sensed crop surface temperatures. Remote Sens. Environ. 9, 27–45.
1098 https://doi.org/10.1016/0034-4257(80)90045-0
1099 Sousa, D., Davis, F.W., 2020. Scalable mapping and monitoring of Mediterranean-climate oak
1100 landscapes with temporal mixture models. Remote Sens. Environ. 247, 111937.
1101 https://doi.org/10.1016/j.rse.2020.111937
1102 Sperry, J.S., Love, D.M., 2015. What plant hydraulics can tell us about responses to
1103 climate- change droughts. New Phytol. 207, 14–27. https://doi.org/doi:10.1111/nph.13354
1104 Tane, Z., Roberts, D., Koltunov, A., Sweeney, S., Ramirez, C., 2018. A framework for detecting
1105 conifer mortality across an ecoregion using high spatial resolution spaceborne imaging
1106 spectroscopy. Remote Sens. Environ. 209, 195–210.
1107 https://doi.org/10.1016/j.rse.2018.02.073
1108 Thompson, D.R., Gao, B.C., Green, R.O., Roberts, D.A., Dennison, P.E., Lundeen, S.R., 2015.
1109 Atmospheric correction for global mapping spectroscopy: ATREM advances for the
1110 HyspIRI preparatory campaign. Remote Sens. Environ. 167, 64–77.
1111 https://doi.org/10.1016/j.rse.2015.02.010

1112 Trugman, A.T., Detto, M., Bartlett, M.K., Medvigy, D., Anderegg, W.R.L., Schwalm, C.,
1113 Schaffer, B., Pacala, S.W., 2018. Tree carbon allocation explains forest drought-kill and
1114 recovery patterns. Ecol. Lett. 21, 1552–1560. https://doi.org/10.1111/ele.13136
1115 United States Census Bureau, 2019. QuickFacts: Santa Barbara city, California [WWW
1116 Document]. URL
1117 https://www.census.gov/quickfacts/fact/table/santabarbaracitycalifornia/PST045218
1118 (accessed 7.10.19).
1119 United States Drought Monitor, 2020. Time Series [WWW Document]. URL
1120 https://droughtmonitor.unl.edu/Data/Timeseries.aspx (accessed 6.19.20).
1121 Ustin, S.L., Roberts, D.A., Gamon, J.A., Asner, G.P., Green, R.O., 2004. Using imaging
1122 spectroscopy to study ecosystem processes and properties. Bioscience 54, 523–534.
1123 van der Linden, S., Okujeni, A., Canters, F., Degerickx, J., Heiden, U., Hostert, P., Priem, F.,
1124 Somers, B., Thiel, F., 2018. Imaging Spectroscopy of Urban Environments. Surv. Geophys.
1125 https://doi.org/10.1007/s10712-018-9486-y
1126 Van der Molen, M.K., Dolman, A.J., Ciais, P., Eglin, T., Gobron, N., Law, B.E., Meir, P., Peters,
1127 W., Phillips, O.L., Reichstein, M., Chen, T., Dekker, S.C., Doubková, M., Friedl, M.A.,
1128 Jung, M., van den Hurk, B.J.J.M., de Jeu, R.A.M., Kruijt, B., Ohta, T., Rebel, K.T.,
1129 Plummer, S., Seneviratne, S.I., Sitch, S., Teuling, A.J., van der Werf, G.R., Wang, G., 2011.
1130 Drought and ecosystem carbon cycling. Agric. For. Meteorol. 151, 765–773.
1131 https://doi.org/10.1016/j.agrformet.2011.01.018
1132 Vicente-Serrano, S.M., Beguería, S., López-Moreno, J.I., 2010. A Multiscalar Drought Index
1133 Sensitive to Global Warming: The Standardized Precipitation Evapotranspiration Index. J.
1134 Clim. 23, 1696–1718. https://doi.org/10.1175/2009JCLI2909.1

1135 Vicente-Serrano, S.M., Gouveia, C., Camarero, J.J., Begueria, S., Trigo, R., Lopez-Moreno, J.I.,
1136 Azorin-Molina, C., Pasho, E., Lorenzo-Lacruz, J., Revuelto, J., Moran-Tejeda, E., Sanchez-
1137 Lorenzo, A., 2013. Response of vegetation to drought time-scales across global land biomes.
1138 Proc. Natl. Acad. Sci. 110, 52–57. https://doi.org/10.1073/pnas.1207068110
1139 Wetherley, E.B., McFadden, J.P., Roberts, D.A., 2018. Megacity-scale analysis of urban
1140 vegetation temperatures. Remote Sens. Environ. 213, 18–33.
1141 https://doi.org/10.1016/j.rse.2018.04.051
1142 Williams, A.P., Seager, R., Abatzoglou, J., Cook, B., Smerdon, J., Cook, E., 2015. Contribution
1143 of anthropogenic warming to California drought during 2012 – 2014. Geophys. Res. Lett. 1–
1144 10. https://doi.org/10.1002/2015GL064924.Received
1145 Williams, A.P., Cook, E.R., Smerdon, J.E., Cook, B.I., Abatzoglou, J.T., Bolles, K., Baek, S.H.,
1146 Badger, A.M., Livneh, B., 2020. Large contribution from anthropogenic warming to an
1147 emerging North American megadrought. Science (80-.). 368, 314–318.
1148 https://doi.org/10.1126/science.aaz9600
1149 Wright, M.N., Ziegler, A., 2017. Ranger: A fast implementation of random forests for high
1150 dimensional data in C++ and R. J. Stat. Softw. 77, 1–17.
1151 https://doi.org/10.18637/jss.v077.i01
1152 Yuan, F., Bauer, M.E., 2007. Comparison of impervious surface area and normalized difference
1153 vegetation index as indicators of surface urban heat island effects in Landsat imagery.
1154 Remote Sens. Environ. 106, 375–386. https://doi.org/10.1016/j.rse.2006.09.003
1155 Zarco-Tejada, P.J., González-Dugo, V., Berni, J.A.J., 2012. Fluorescence, temperature and
1156 narrow-band indices acquired from a UAV platform for water stress detection using a
1157 micro-hyperspectral imager and a thermal camera. Remote Sens. Environ. 117, 322–337.
1158 https://doi.org/10.1016/j.rse.2011.10.007

1159 Zhou, Q., Xian, G., Shi, H., 2020. Gap fill of land surface temperature and reflectance products in
1160 landsat analysis ready data. Remote Sens. 12, 1–16. https://doi.org/10.3390/rs12071192
1161 Ziter, C.D., Pedersen, E.J., Kucharik, C.J., Turner, M.G., 2019. Scale-dependent interactions
1162 between tree canopy cover and impervious surfaces reduce daytime urban heat during
1163 summer. Proc. Natl. Acad. Sci. 201817561. https://doi.org/10.1073/pnas.1817561116

Supplementary Data

Click here to download Supplementary Data: miller_etal_rse_veg_drought_response_dynamics_supplemental.docx

***Declaration of Interest Statement**

Declaration of interests

☒ The authors declare that they have no known competing financial interests or personal relationships that could have appeared to influence the work reported in this paper.

☐The authors declare the following financial interests/personal relationships which may be considered as potential competing interests:

Credit Author Statement

David L. Miller: Conceptualization, Methodology, Software, Validation, Formal Analysis, Investigation, Data Curation, Writing – Original Draft, Writing – Review and Editing, Funding Acquisition

Michael Alonzo: Validation, Resources, Data Curation, Writing – Original Draft, Writing – Review and Editing

Susan K. Meerdink: Validation, Resources, Data Curation, Writing – Original Draft, Writing – Review and Editing

Michael A. Allen: Visualization, Writing – Original Draft, Writing – Review and Editing

Christina L. Tague: Conceptualization, Methodology, Writing – Original Draft, Writing – Review and Editing

Dar A. Roberts: Conceptualization, Methodology, Validation, Resources, Data Curation, Writing – Original Draft, Writing – Review and Editing

Joseph P. McFadden: Conceptualization, Methodology, Resources, Writing – Original Draft, Writing – Review and Editing, Funding Acquisition